GEOPERSIA

Accepted Manuscript

Assessment and Prediction of Rock Drillability in Hard Granitic Rocks Using Experimental Testing and Machine Learning Models

Ebrahim Sharifi Teshnizi, Mohammad Ghafoori, Gholam Reza Lashkaripour, Jafar Khademi Hamidi, Amir Hossein Yousefi

DOI: 10.22059/geope.2026.401662.648840

Receive Date: 01 September 2025
Revise Date: 15 January 2026
Accept Date: 24 January 2026

Assessment and Prediction of Rock Drillability in Hard Granitic Rocks Using Experimental Testing and Machine Learning Models

Ebrahim Sharifi Teshnizi [1, *], Mohammad Ghafoori [1], Gholam Reza Lashkaripour [1], Jafar Khademi Hamidi [2], Amir Hossein Yousefi [3]

[1] Department of Geology, Faculty of Science, Ferdowsi University of Mashhad, Mashhad, P.O. Box 91775-1436, Iran
[2] Department of Mining Engineering, Faculty of Engineering, Tarbiat Modares University, Tehran, Iran
[3] Department of Civil Engineering, Shahi.C., Islamic Azad University, Shahinshahr, Iran

Received: 01 September 2025, Revised: 15 January 2026, Accepted: 24 January 2026

Abstract
Accurate prediction of rock drillability is critical for optimizing tunneling, mining, and excavation operations in hard rock environments. This study investigates the drillability of granitic rocks by integrating petrographic, physical, mechanical, and abrasivity parameters with both conventional regression and machine learning (ML) approaches. Laboratory tests were conducted on samples from six granitic rock groups, measuring properties such as brittleness, hardness, abrasivity indices, and the Drilling Rate Index (DRI). Statistical analyses, including linear and nonlinear regression, revealed strong nonlinear relationships between DRI and engineering parameters, with R^2 values up to 0.95. Machine learning models, particularly Random Forest (RF) and Artificial Neural Networks (ANN), were applied independently, with RF achieving superior predictive performance ($R^2 > 0.99$) and lower error indices compared to ANN and regression models. The study also highlights the influence of different rock groups on model performance and discusses limitations related to dataset scale, in situ conditions, and model generalization. These results confirm that integrating laboratory measurements with ML techniques provides a reliable framework for predicting rock drillability, offering practical guidance for excavation planning, equipment selection, and operational efficiency.

Keywords: Granitic rocks, Drilling Rate Index (DRI), Machine Learning, Random Forest, Artificial Neural Networks, Rock drillability, Abrasivity, Rock mechanics.

Introduction

Efficient excavation in igneous rocks requires accurate prediction of drillability, commonly quantified by the Drilling Rate Index (DRI). Tunnel design and construction involve a complex interplay of technical and economic decisions that evolve throughout the design and execution phases. These decisions are shaped by the collaborative efforts of the owner, designer, and construction company, and are heavily influenced by preliminary geological knowledge and the development of site-specific conditions (Peila & Pelizza, 2009). When employing a rock tunnel boring machine (TBM), its performance is largely dictated by the properties of the rock mass. A “limiting situation” arises when the TBM cannot operate as intended due to geological challenges, resulting in reduced advance rates or complete obstruction (Pelizza & Peila, 2001; Peila & Pelizza, 2009, Karrari et. al., 2023, Yang et. al., 2025, Wu et. al., 2025). These limitations are not absolute but are relative to the TBM’s design and operational parameters.

* Corresponding author e-mail: Ebrahim.SharifiTeshnizi@mail.um.ac.ir

Common limiting conditions include poor borability, low drillability, tunnel face instability, fault zones, groundwater inflow, clay-rich soils, high temperatures, gas pockets, and karstic cavities.

Drillability, a critical factor in excavation efficiency, refers to the penetration rate and tool wear during drilling operations (Thuro & Spaun, 1996; Köhler et al., 2011). It is influenced by both controllable parameters–such as thrust force, bit type, and rotational speed–and uncontrollable rock properties. Accurate prediction of drillability is essential for cost estimation, equipment selection, and project scheduling. However, no single parameter can fully define drillability (Altindag, 2004). While uniaxial compressive strength (UCS) is the most commonly used predictor (Paone & Madson, 1966; Paone et al., 1966; Fowell & McFeat-Smith, 1976; Poole & Farmer, 1978; Aleman, 1981; Karpuz et al., 1990; Akcin et al., 1994; Bilgin et al., 1996; Huang & Wang, 1997; Kahraman, 1999; Kahraman et al., 2003; Tanaino, 2005; Akun & Karpuz, 2005, Motamed-Shariati et al., 2023), other parameters such as tensile strength, quartz content, porosity, and P-wave velocity also play significant roles (Howarth et al., 1986; Akcin et al., 1994; Kahraman, 1999). A wide array of empirical indices—including Schmidt rebound hardness, point load strength, Shore hardness, Taber abrasion, Cerchar abrasivity index (CAI), specific energy (SE), texture coefficient (TC), and drilling rate index (DRI)–have been developed to estimate drilling performance (McFeat-Smith & Fowell, 1977; Kovscek et al., 1988; Kahraman et al., 2003, Wani, et.al. 2025).

Despite the prevalence of strength-based predictors, recent studies emphasize the importance of mineralogical and petrographic features in determining rock behavior. Rocks are composed of varying proportions of minerals with diverse grain sizes, shapes, and microfabric characteristics, which significantly influence their mechanical performance (Aligholi et al., 2018). Investigations have shown that properties such as grain interlocking, orientation, porosity, and boundary conditions affect strength and drillability (Howarth & Rowlands, 1987; Akesson et al., 2003; Prikryl, 2006; Tandon & Gupta, 2013; Ajalloeian & Kamani, 2017; Karrari et.al., 2025, Hashemi et.al., 2025). Quantitative approaches to petrographic characterization have gained traction, linking mineral grain size and shape to mechanical indices like UCS, tensile strength, and hardness (Yilmaz et al., 2011; Moradizadeh et al., 2016; Sajid et al., 2016; Akram et al., 2017; Comakli & Cayirli, 2018; Hemmati et al., 2020, Zhou et. al., 2025).

Studies have also demonstrated that grain size has a more pronounced effect on rock strength than mineral content alone. For instance, larger quartz grain sizes correlate negatively with UCS, while feldspar grain size impacts tensile strength and ultrasonic velocity (Yilmaz & Kahraman., 2011; Sajid et al., 2016). Models incorporating equivalent quartz content (EQC) and UCS have proven effective in predicting CAI values (Rostami et al., 2014; Capik & Yilmaz, 2017). However, contradictory findings exist, highlighting the complexity of these relationships (Alber & Kahraman, 2009; Prikryl, 2006). Microscale features such as cement matrix, pore structure, and texture coefficient have also been linked to cuttability and drillability indices (Rostami et al., 2020). While TC is a useful parameter, it does not account for anisotropy due to foliation or microfractures, prompting the development of alternative indices like the heterogeneity index (Villeneuve, 2008; Peng et al., 2017, Ezazi et al., 2024).

Table 1 outlines the potential correlations between the Drilling Rate Index (DRI) and various rock properties. These encompass fundamental geotechnical characteristics such as rock strength (represented by UCS, BTS, and IS_{50}), a range of brittleness measures (B_1, B_2, B_3, B_4, B_5, B_8, and B_{10}), hardness (including SRH, SSH, LH, and SH), as well as density and porosity. However, the specific focus of this investigation is on abrasivity properties—namely the Rock Abrasivity Index (RAI), the Abrasivity Index (ABI), and the CERCHAR Abrasivity Index (CAI)–and mineralogical properties, which include Vickers hardness (VHNR) and equivalent quartz content (EQC). This focus is driven by the fact that prior studies have largely neglected

the influence of mineralogical properties on drillability.

Rock drillability is a key factor in rock engineering, mining, and tunneling operations, and as a result, considerable research efforts have been devoted to estimating drilling and penetration performance. Numerous recent studies have proposed empirical, statistical, and data-driven approaches to model drilling behavior (Ataei et al., 2015; Fattahi and Bazdar, 2017; Koopialipoor et al., 2019; Darbor et al., 2019; Ru et al., 2019; Zhou et al., 2020; Srivastava and Vemavarapu, 2021; Keller et al., 2023; Ren et al., 2024; Karrari et.al., 2024; Bertini and Lavi, 2025).

In recent years, soft computing techniques have increasingly been adopted as effective alternatives to traditional statistical methods, particularly due to their ability to address uncertainty, imprecision, and complex nonlinear relationships. Table 2 provides an overview of previous studies that have applied machine learning algorithms for the estimation of the Drilling Rate Index (DRI), highlighting their effectiveness in drillability prediction. The table shows that a wide range of machine learning techniques has been employed for DRI estimation across different studies, reflecting the growing interest in data-driven approaches for modeling rock drillability.

Table 1. Relationships between Drilling Rate Index (DRI) and rock properties

Correlation with DRI	R^2	Rock type	Investigators
$DRI = 55.69 + 77.16 \exp(-0.0005\ B_8)$	0.73	Sedimentary, Metamorphic, and Igneous	Yarali and Kahraman (2011)
$DRI = -0.264\ UCS + 87.049$	0.71	Sedimentary, Metamorphic, and Igneous	Yarali and Soyer (2013)
$DRI = -2.798\ BTS + 85.674$	0.55		
$DRI = -0.983\ SRH + 118.43$	0.78		
$DRI = -0.577\ SSH + 91.652$	0.64		
$DRI = -5.872\ IS_{50} + 86.297$	0.71		
$DRI = 191.62\ UCS^{-0.292}$	0.79	Sedimentary, and Metamorphic	Ekincioglu and et al. (2013)
$DRI = 120.95\ BTS^{-0.489}$	0.87		
$DRI = -27.6\ LN\ (IS50) + 92.333$	0.83		
$DRI = 82.705 - 0.224\ UCS$	0.84	Sedimentary, Metamorphic, and Igneous	Ozfirat et al. (2016)
$DRI = 84.764 - 2.7497\ BTS$	0.78		
$DRI = 73.609 - 0.0269\ B8$	0.81		
$DRI = 84.151 - 0.4455\ B10$	0.84		
$DRI = 340 - 0.23UCS - 94\ P$	0.74	Granite, basalt	Yenice et al. (2018)
$DRI = -89.96 + 2.33UCS\text{-}0.009UCS2$	0.93		
$DRI = -2.31BTS2 + 46.14BTS\text{-}162.78$	0.72		
$DRI = -140.19VP + 429.87$	0.42		
$DRI = -0.29\ UCS + 98.12$	0.57	Sedimentary, Metamorphic, and Igneous	Yenice (2019)
$DRI = 80.13 - 0.0078UCS - 2.978BTS$	0.34		
$DRI = 109.2 - 0.243UCS - 1.734BTS$	0.66		
$DRI = 104.4 - 0.407UCS - 3.043BTS$	0.78		
$DRI = -0.8253SH + 93.364$	0.95	Sedimentary, and Metamorphic	Ekincioglu and Akbay (2021)
$DRI = -0.1778LH + 155.46$	0.96		
$DRI = -1.2321SCH + 102.89$	0.86		
$DRI = 26.80 + 18.42\ n$	0.613	Granite	Karrari er. al. (2022)
$DRI = 63.83 - 0.22\ UCS$	0.829		
$DRI = 71.20 - 4.24\ IS50$	0.742		
$DRI = 102.05 - 17.20\ LN\ (E)$	0.601		
$DRI = 149.15 - 12.83\ LN\ (RAI)$	0.413		
$DRI = 63.30 - 0.033\ ABI$	0.775		
$DRI = 79.55 - 38.14\ LN\ (CAI)$	0.565		

UCS uniaxial compressive strength, BTS Brazilian tensile strength, brittleness value ($B_1 = UCS / BTS$, $B_2 = (UCS\text{-}BTS)/(UCS + BTS)$, $B_3 = (UCS \times BTS)/2$, $B_4 = \sqrt{B_3}$, $B_5 = (UCS \times BTS)\ 0.72$, $B_8 = (UCS \times BTS)/2$, $B_{10} = (UCS + BTS)/2$), SRH Schmidt rebound hardness, SSH Shore Scleroscope hardness, P density, n porosity, SH Shore hardness, IS50 point load index, DRI act drilling rate index actual, DRI pre drilling rate index prediction, LH Leeb hardness, SCH Schmidt hardness

Jang and Topal (2014) provided a comprehensive review of soft computing applications in mining engineering, highlighting their effectiveness in solving problems such as mining method selection, equipment selection, and performance prediction. Given that natural processes are inherently nonlinear and that the Drilling Rate Index (DRI) is influenced by multiple interacting rock properties, nonlinear modeling approaches with multiple explanatory variables are better suited to realistically quantify drillability (Zielesny, 2016; Nisbet et al., 2018). Zielesny (2016) further emphasized that, to avoid scientific bias, no prior assumptions should be imposed on the form of these nonlinear relationships.

Consequently, a wide range of advanced modeling techniques has been explored in the literature. Ataei et al. (2015) proposed a new penetration rate model and evaluated its performance against existing empirical formulations. Fattahi and Bazdar (2017) developed hybrid ANN models optimized using metaheuristic algorithms such as simulated annealing, firefly algorithm, invasive weed optimization, and shuffled frog leaping to estimate DRI. Koopialipoor et al. (2019) introduced a deep neural network model for penetration rate prediction, demonstrating improved performance over conventional ANN approaches. Darbor et al. (2019) compared multiple regression techniques with multilayer neural networks, confirming the superiority of nonlinear models for penetration rate estimation.

More advanced hybrid and evolutionary techniques have also been investigated. Ru et al. (2019) integrated Monte Carlo simulation with least-squares support vector machines to predict DRI under uncertainty. Zhou et al. (2020) applied ANN and genetic programming to estimate tunnel boring machine performance. Srivastava and Vemavarapu (2021) developed a composite penetration rate index and validated it using regression analysis. Recently, Keller et al. (2023) evaluated various machine learning models for real-time penetration rate prediction, while Ren et al. (2024) proposed an adaptive feature-optimized methodology to enhance prediction accuracy. Bertini and Lavi (2025) compared data-stream learning algorithms with traditional machine learning models for penetration rate estimation.

Despite these advances, most existing studies focus primarily on operational or mechanical parameters and often neglect the combined influence of petrographic characteristics, abrasivity indices, and mineralogical composition. Moreover, many machine learning-based models are developed for single lithological settings and do not explicitly examine the effect of different rock groups on model performance. These limitations highlight the need for integrated modeling frameworks that incorporate comprehensive laboratory-based rock properties and evaluate model robustness across multiple rock types, which forms the primary motivation of the present study.

The novelty of this study lies in the integration of petrographic, mechanical, physical, and abrasivity properties with advanced machine learning models (ANN and RF) to predict the Drilling Rate Index (DRI) in granitic rocks. Unlike previous studies, which typically focus on single rock properties or employ conventional regression, this work applies ANN and RF independently to six distinct granitic rock groups, enabling the evaluation of lithology-specific influences on drillability. Furthermore, regression analysis is used to identify statistically significant parameters (e.g., H, S_J, S_{20}) that dominate DRI, improving interpretability and scientific rigor.

To the best of our knowledge, this study represents the first integrated multi-parameter, multi-rock-group, and dual-model approach for DRI estimation in granitic rocks. The proposed approach demonstrates higher predictive accuracy and generalization capability compared to traditional methods and provides a comprehensive framework for predicting rock drillability in practical engineering applications, including tunneling, mining, and excavation planning.

Overview of the Geological Study of Kani Sib Water-Conveyance Tunnel (KSWCT)

The Kani Sib Water-Conveyance Tunnel (KSWCT) is a major hydraulic engineering project

designed to transfer water from the Kani Sib Dam to Lake Urmia in West Azerbaijan Province, Iran (Figure 1) (Sadeghi, et. al., 2024). The tunnel has an internal diameter of 6.32 m and was excavated using a double-shield hard-rock Tunnel Boring Machine (TBM) manufactured by the NFM–NHI group. A 20.3 km long northeastern section of the tunnel was driven through extremely hard and highly abrasive granitic rock formations, which created severe operational difficulties, particularly related to rapid disc cutter wear and reduced excavation efficiency (Figures 2 and 3).

Table 2. Summary of applications of ML algorithms for estimating CAI in different engineering fields

No.	Data size	Input parameters	Output parameter	Application field(s)	ML algorithm(s)[a]	Best ML algorithm	Performance [b]	Key findings	Investigators
1	63 samples	UCS, BTS, density, brittleness, bit diameter, RPM, thrust	Drilling Rate (DR)	Diamond core drilling (mining, geotechnical)	ANN, ANFIS, GA-ANN, ML regression	Non-linear multiple regression	R = 0.87 (diamond), R = 0.85 (percussion)	Non-linear multi-variable models outperform simple regression; BI, density, UCS, and machine specs are critical.	Yazitova & Yagiz (2024)
2	37 samples	Mineralogy, texture coefficient, grain size, UCS, BTS, SSH, CAI, Poisson's ratio	Drilling Rate Index (DRI)	Natural stone quarrying (mining, construction)	GEP-PSO, regression analysis	GEP-PSO hybrid model	R^2 = 0.84–0.90, MSE = 4.86–9.83	Texture coefficient and grain size significantly influence DRI; hybrid evolutionary algorithms improve prediction accuracy.	Tumac et al. (2023)
3	20 rock samples	Uniaxial compressive strength (σ_0), Tensile strength (σ_x), Brittleness indices (B_1, B_2, B_3, B_{nen}), Shore hardness, Density	Drilling Rate Index (DRI)	Mining, Tunnelling	Artificial Neural Networks (ANN), Multiple Regression (Linear, 2nd Degree Polynomial)	ANN with Levenberg – Marquardt training	R^2 up to 99.8% in regression, ANN achieved R^2 > 98% across most configurations	DRI depends on complex, nonlinear interactions; ANN outperformed linear and polynomial regression models.	Yetkin et al. (2025)
4	57 datasets	UCS, BTS, S_{20}, S_j, MR, SH, n, SFA, EQC	Drilling Rate Index (DRI)	Mining, Geology, Rock Engineering	GWO-SVM, GWO-RF, GWO-XGBoost	GWO-XGBoost	R^2 = 0.999, MAE ≈ 0.0004, RMSE ≈ 1.81, SI ≈ 0.031	Hybrid GWO-XGBoost model achieved near-perfect prediction accuracy; outperformed GWO-SVM and GWO-RF.	Shahani et al. (2024)

[a] ANN (Artificial Neural network); DE (Differential evolution); DT (Decision tree); GB (Gradient boosting); GBR (Gradient boosting); GEP (Gene expression programming); GPR (Gaussian process regression); KNN (k-nearest neighbour); MLR (Multiple linear regression); MVRA (Multi-variate regression analysis); PSO (Particle swarm optimization);RF (Random forest); RFR (Random forest regressor); RT (Regression tree); SA (Simulated annealing); SVR (Support vector regressor); XGB (Extreme gradient boosting).

[b] R (Coefficient of correlation); R^2 (Coefficient of determination); RMSE (Root mean squared error)

The exceptional hardness and abrasiveness of the granite made this tunnel section an ideal case study for evaluating rock mass behavior and boring performance indices, especially the Drilling Rate Index (DRI). Understanding these relationships is critical for predicting TBM performance, optimizing cutterhead design, improving tool life, and reducing construction time and operational costs.

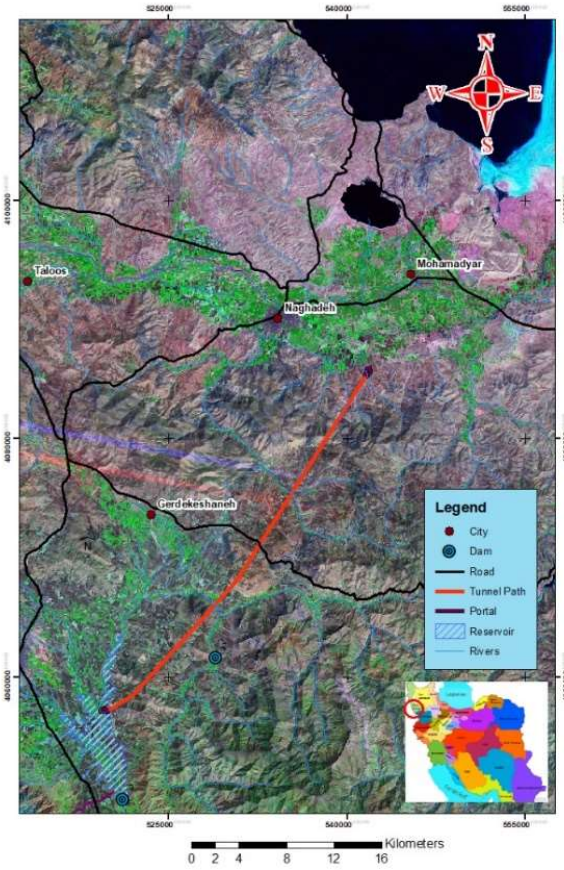

Figure 1. Location map of the KSWCT project study area

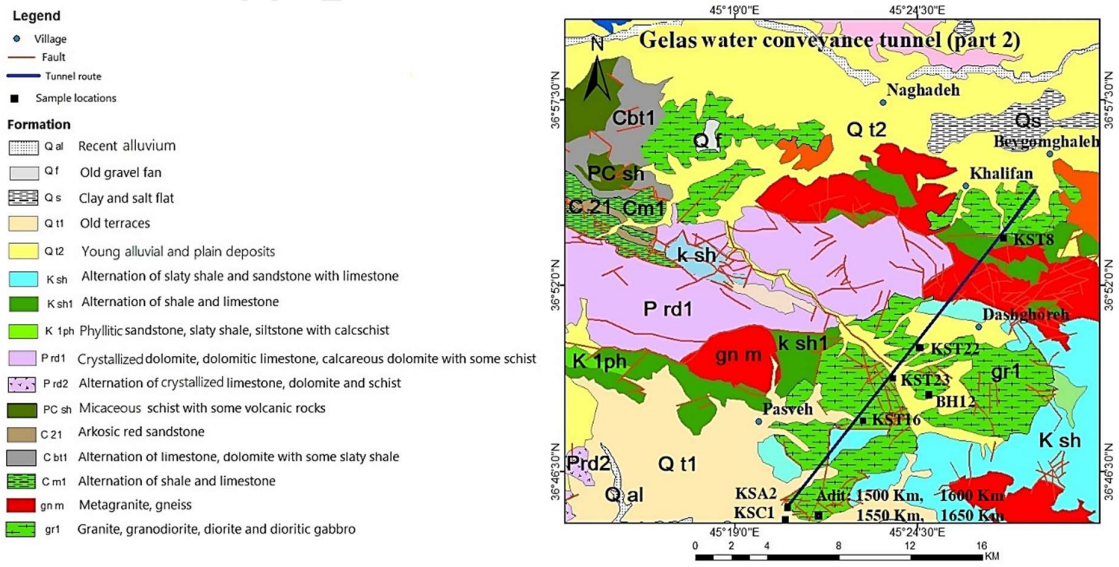

Figure 2. Geological map of the KSWCT project study area

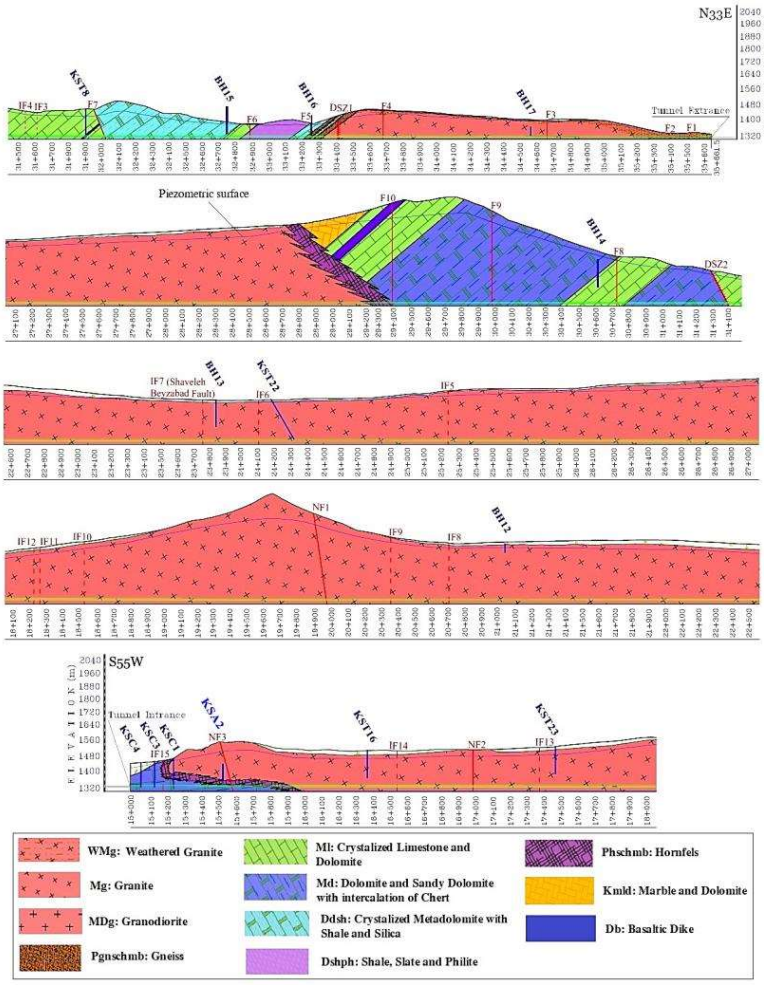

Figure 3. Cross-section showing engineering geology along 20.3-km-long northeast section of the KSWCT alignment

This study focuses on establishing quantitative relationships between the engineering properties of granitic rocks, their petrographic and mineralogical characteristics, and the Drilling Rate Index (DRI). For this purpose, a total of 41 granitic rock samples were collected from 41 different locations along the KSWCT alignment in Naghadeh City, West Azerbaijan Province. Laboratory tests were conducted to determine physical and mechanical properties such as uniaxial compressive strength (UCS), Brazilian tensile strength (BTS), point load index (IS_{50}), density, porosity, and abrasivity. In parallel, detailed petrographic analyses were performed using thin-section microscopy to evaluate mineral composition, grain size, texture, and fabric. The resulting dataset was then statistically analyzed to develop predictive models for DRI and to assess the influence of mineralogical and textural features on drilling performance.

The findings of this research provide valuable insights for future tunneling projects in hard and abrasive rock conditions and contribute to more reliable prediction of TBM advance rates in similar geological environments.

Methodology

This study employed a two-pronged methodology to estimate the DRI of igneous rocks, combining experimental laboratory tests with ensemble machine learning (ML) algorithms**.** The detailed flowchart of the research methods used in this study is presented in Figure 4.

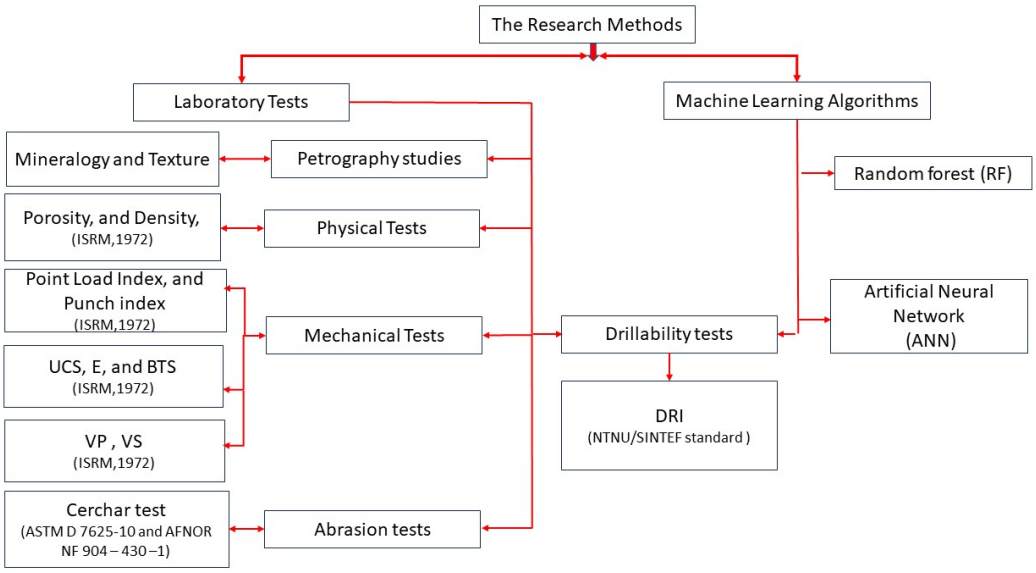

Figure 4. Detailed flowchart of the research methods

Experimental investigation

Figure 5 presents representative images of the rock blocks used in this study. The sampling procedure followed the recommendations of the ISRM (2007) guidelines. Both unweathered and slightly weathered rock materials were collected to ensure that the dataset captured the natural variability of the formations. During sampling, particular attention was given to selecting blocks with homogeneous physical characteristics and without visible fractures, discontinuities, or weakness planes that could compromise the reliability of the laboratory results. Additional inspections were also carried out during core extraction to verify that the internal structure of each specimen remained intact and suitable for detailed testing.

For the preparation of test specimens, cylindrical cores with diameters of 54 mm and 100 mm were drilled from the selected blocks. The ends of the cores were then cut using a rock saw and subsequently ground to produce smooth, parallel surfaces appropriate for mechanical and physical testing. The full sequence of coring, trimming, and polishing is illustrated in Figure 5, along with an overview of the prepared cores.

A comprehensive experimental program was conducted on all specimens (Figures 4 and 5). Petrographic analyses were carried out to determine mineralogical composition and textural characteristics, while a series of physical and mechanical tests were performed to evaluate fundamental rock properties. The Cerchar Abrasivity Index (CAI) and drillability tests were included to assess the abrasive behavior of the rock and its performance during mechanical excavation. Detailed descriptions of these experimental procedures are provided in the following sections.

All rock core specimens and laboratory tests were performed in accordance with ISRM (2007) recommendations. The physical and mechanical tests included porosity (n), density (ρ), Brazilian tensile strength (BTS), uniaxial compressive strength (UCS), point load index (Is_{50}), wave velocity (V_p and V_s), Schmidt hammer hardness (SH), and punch strength index (P_d). The Cerchar Abrasivity Index (CAI) test followed the method proposed by Alber et al. (2014). In addition, the Drilling Rate Index (DRI) test was conducted in accordance with the methodology developed at the Norwegian University of Science and Technology (NTNU), as described by Nilsen (2003). A summary of all tests performed, including sample numbers and associated testing standards, is given in Table 3. Adhering to these standardized procedures ensured the consistency, accuracy, and comparability of the results obtained in this study.

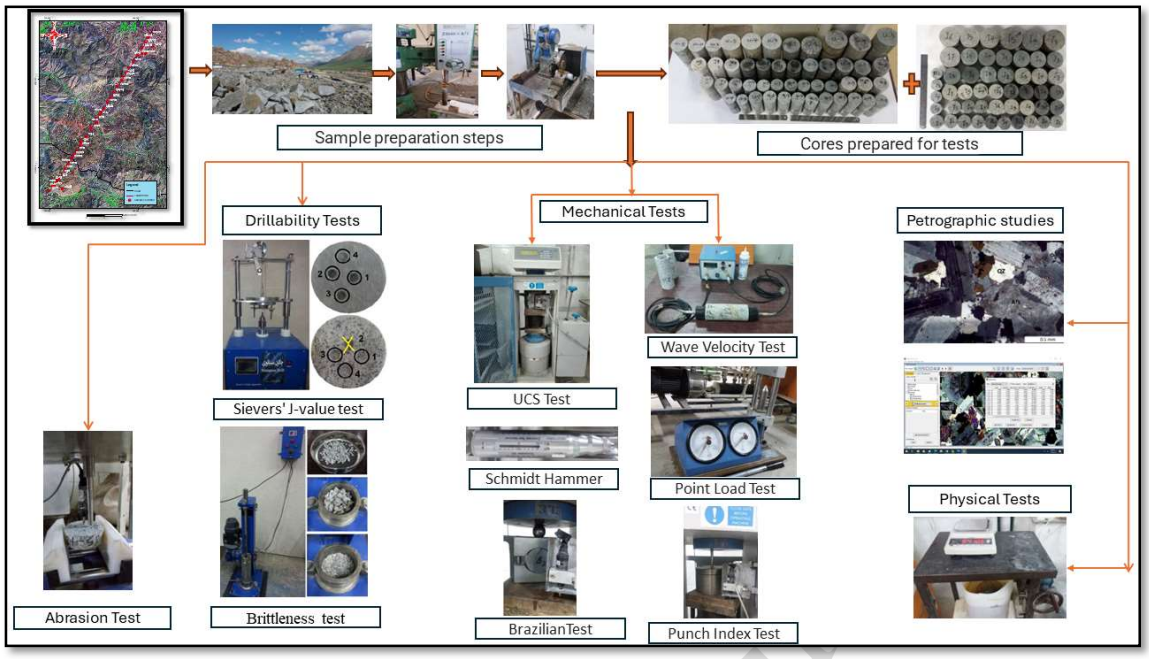

Figure 5. Sample preparation workflow and overview of the comprehensive testing program

Table 3. Summary of Test Types, Test Counts, and Corresponding Standards

Test name	Minimum Number of Tests Required by Standard	Standard
Physical tests (n, ρ)	5	ISRM (2007)
BTS, SH, and IS_{50}	10	ISRM (2007)
UCS, V_P, V_S, P_d, and CAI	5	ISRM (2007)
DRI	5	Nilsen (2003)

Ensemble ML algorithms

This study employs two machine learning models-Artificial Neural Networks (ANN) and Random Forest (RF)-to predict the Drilling Rate Index (DRI) of igneous rocks. The models were applied independently, and their performances were subsequently compared to evaluate their relative predictive capabilities.

The selection of ANN and RF was motivated by their well-established ability to model complex and nonlinear relationships commonly encountered in geotechnical datasets. ANN models are particularly effective for relatively small datasets with high-dimensional input spaces, as they can capture hidden nonlinear patterns and provide robust generalization. In contrast, RF models are known for their strong resistance to overfitting and their capability to handle multicollinearity through ensemble learning and random feature selection.

Prior to models used, extensive data cleaning and preprocessing procedures were performed, including consistency checks, normalization of input variables, and outlier evaluation, to ensure data reliability and model stability. Both ANN and RF models were trained and tested using the same preprocessed dataset to enable a fair and consistent performance comparison.

The complete workflow of the adopted machine learning methodology, from data preparation to model evaluation, is illustrated in Figure 6. This section presents the theoretical background of the ANN and RF approaches and clarifies their individual roles in accurately predicting rock drillability.

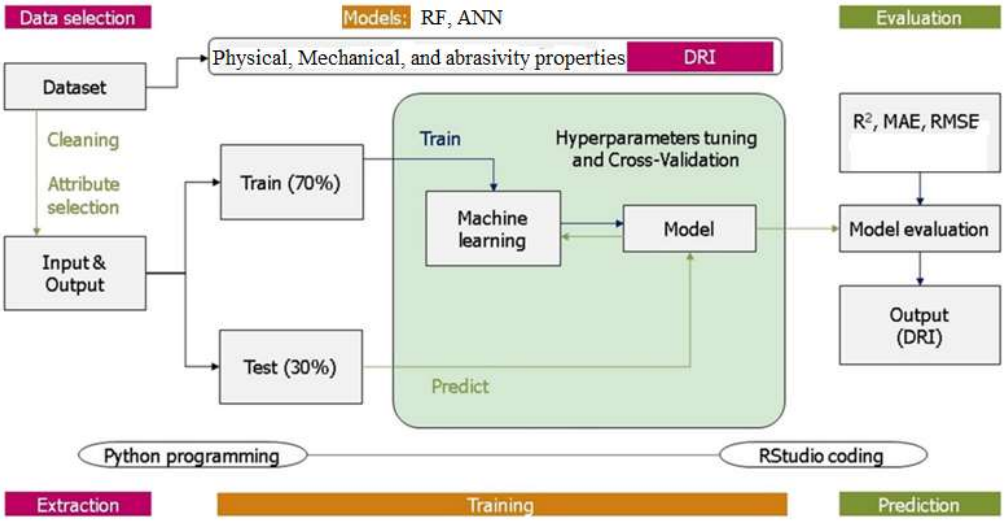

Figure 6. Systematic and optimized machine learning workflow adopted for DRI prediction, including data preprocessing, independent ANN and RF model development, and performance evaluation

Random Forest (RF)

This study utilized an ensemble ML algorithm namely extreme random forest (RF) for prediction of Drilling Rate Index (DRI) of igneous rocks. The rationale for selecting this ensemble ML algorithm stems from its proven ability to handle complex, non-linear relationships within small to moderately sized datasets. This model is robust to multicollinearity, allows feature importance evaluation, and generally provides high accuracy with reduced overfitting. Given the limited and heterogeneous nature of the experimental dataset, ensemble techniques offer an optimal balance between predictive performance and generalizability (Ergen & Katlay,. 2024, Tabar, et.al. 2025). In the present study, the development of models was predominantly performed using Python programming language.

In this RF algorithm, the original dataset undergoes resampling to generate numerous samples, typically using the bootstrap method. Subsequently, regression trees are created for each bootstrap sample, and the final results are determined through voting, integrating the predictions of the classification trees. RF can be used for both regression and classification tasks (Dai, et.al. 2018). The RF model is an ensemble technique that combines multiple independent classification trees (Huang et.al. 2020). The prediction probability is calculated based on the proportion of trees that voted for a particular class. To validate the model, out-of-bag (OOB) samples are employed. Afterward, the overall error for each decision tree is calculated to assess its performance (Farooq et. al. 2020, Wang et.al. 2025).

Artificial Neural Network (ANN)

An Artificial Neural Network (ANN) is a computational model that learns to recognize inherent patterns and relationships within a dataset. Through a process called training, the network acquires knowledge from this data and stores it within its internal structure (connection weights), allowing it to generalize this knowledge to new, similar cases. This experiential learning process is analogous to the human brain in two key aspects (Haykin & Lippmann, 1994, Rastegarnia et.al. 2018, 2021, Rahimi et.al. 2019):

- Knowledge is acquired through a iterative training process.
- Information is stored internally through the strength of connections between nodes, mirroring

the synaptic strength in biological neural networks.

Structurally, neural networks are categorized as either single-layer or multi-layer. Multi-layer networks, which are essential for solving complex problems, consist of three fundamental types of layers. The basic processing units within these layers are called neurons. In a standard architecture, each neuron in a given layer is connected to every neuron in the adjacent layers, but not to other neurons within its own layer. A multi-layer network comprises an input layer, one or more hidden layers, and an output layer. Data is fed into the input layer, processed through the hidden layers, and the final result is produced by the output layer. The hidden layers are not directly exposed to the external input or output data.

An ANN is a logical structure of interconnected elements (neurons) that communicate via adjustable connection weights. These weights are iteratively modified during the training phase to minimize error. The user defines the network's architecture, including the number of hidden layers and the number of neurons in each layer. The network operates through a series of transfer functions that multiply input values by their corresponding connection weights and sum them to produce an output.

Experimental Results

Petrography studies

Petrographic analysis was conducted to quantify mineralogical composition and textural characteristics of the igneous rock samples. For each rock type, five thin sections were prepared in perpendicular and parallel orientations relative to the core axis, enabling comprehensive evaluation of fabric features. Mineral abundance and textural attributes were determined via modal analysis using a Leitz Orthoplan microscope equipped with an automatic point counter and digital imaging system. Following the point-count method (Streckeisen A ,1976), the volumetric proportions of quartz, plagioclase, K-feldspar, biotite and accessory minerals were systematically measured across each thin section. High-resolution images of the entire sample were captured under cross-polarized light (XPL) using Red–Green–Blue color (RGB) filters, preserving textural details in JPG format. To ensure statistical robustness, 50–200 grains per thin section were analyzed, as recommended by (ISRM, 1981). Given the labour-intensive nature of textural quantification, representative sub-regions exhibiting homogeneous mineralogical and structural features were selected for detailed grain boundary tracing and quantification. Full-section mineral counts were further validated using a given protocol (ISRM , 2007), ensuring accuracy across the entire sample area.

The modal composition of the constituent minerals was quantified by calculating the percentage of area occupied by each mineral within the reference section (Table 4). The proportions of the primary rock-forming minerals-quartz, alkali feldspar, plagioclase, and biotite–were subsequently used to classify and name the samples petrographically (Figure 7), following the IUGS classification scheme of Streckeisen (1976). Muscovite, amphibole, chlorite, and opaque phases were identified as accessory or heavy minerals.

Quartz content ranges from 6.97% to 30%, while alkali feldspar and plagioclase vary between 11.00-52.75% and 6.06-45.00%, respectively. These modal proportions indicate that the studied granitic rocks fall within the felsic category. According to Maitre (2002), felsic rocks are typically light-colored and commonly exhibit fine- to medium-grained textures.

The mineral constituents of the samples were quantified by counting grain occurrences in thin sections examined under a polarizing microscope. The procedure involved several steps: (1) capturing high-resolution images using a digital microscope, (2) preparing and refining the images for analysis, (3) extracting key petrographic features, and (4) applying regression analysis to obtain accurate mineralogical and textural parameters.

Table 4. Results of mineralogy and petrography studies of samples

Number of samples	Mineralogy (%)	Microphotograph of samples	Petrographic name
26	Qz: 18.43 Pl: 28.46 Afs: 42.65 Bt: 6.33 Ms: 0 Am: 1.00 Chl: 3.00 Op: 0.13	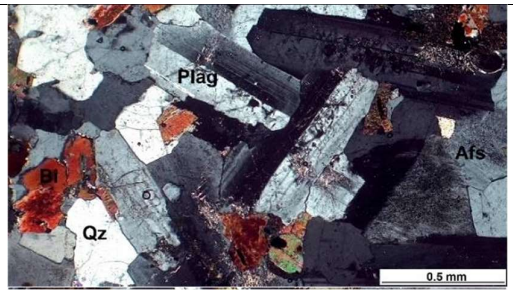	Monzogranite
5	Qz: 11.16 Pl: 20.76 Afs: 42.16 Bt: 8.86 Ms: 13.34 Am: 1.00 Chl: 1.00 Op: 1.71		Quartz syenite
8	Qz: 12.70 Pl: 14.30 Afs: 30.72 Bt: 26.21 Ms: 12.13 Am: 1.50 Chl: 1.00 Op: 1.44	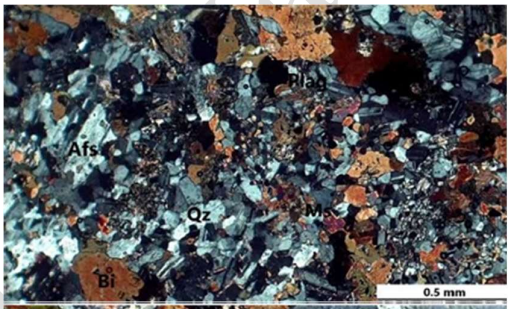	Syenogranite
1	Qz: 12.73 Pl: 30.75 Afs: 38.38 Bt: 15.10 Am: 1.50 Chl: 1.50 Op: 0.06	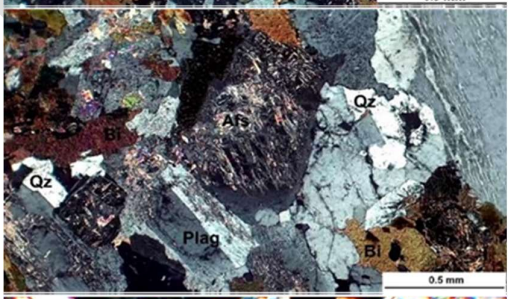	Quartz monzonite
1	Qz: 39.2 Pl: 26.3 Afs: 12.0 Bt: 10.5 Ms: 5 Am: 1.0 Chl: 2.0 Op: 4.0		Granodiorite

NOTE: According to optical microscopy analysis (Streckeisen ,1976), *Qz: quartz; Pl: plagioclase; Afs: Alkali feldspar; Bt: biotite; Muscovite; Am: Amphibole; Chl: chlorite; Op: opaque minerals

Microscopic images of the thin sections were analyzed using JMicro-Vision software (version 1.27). Figure 8 illustrates the procedure used within JMicro-Vision to compute the Texture Coefficient (TC). This open-source image-processing software supports both manual and automated operations, enabling efficient measurement and quantification of petrographic characteristics.

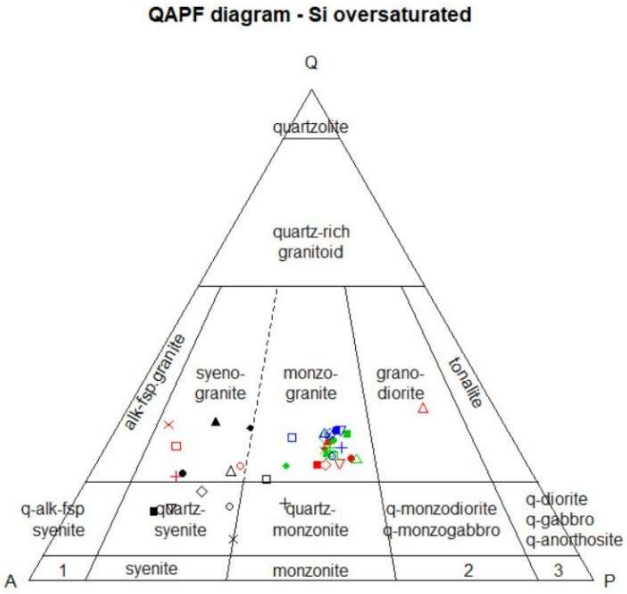

Figure 7. Petrographic classification of the analyzed rock samples based on the IUGS diagram of Streckeisen (1976)

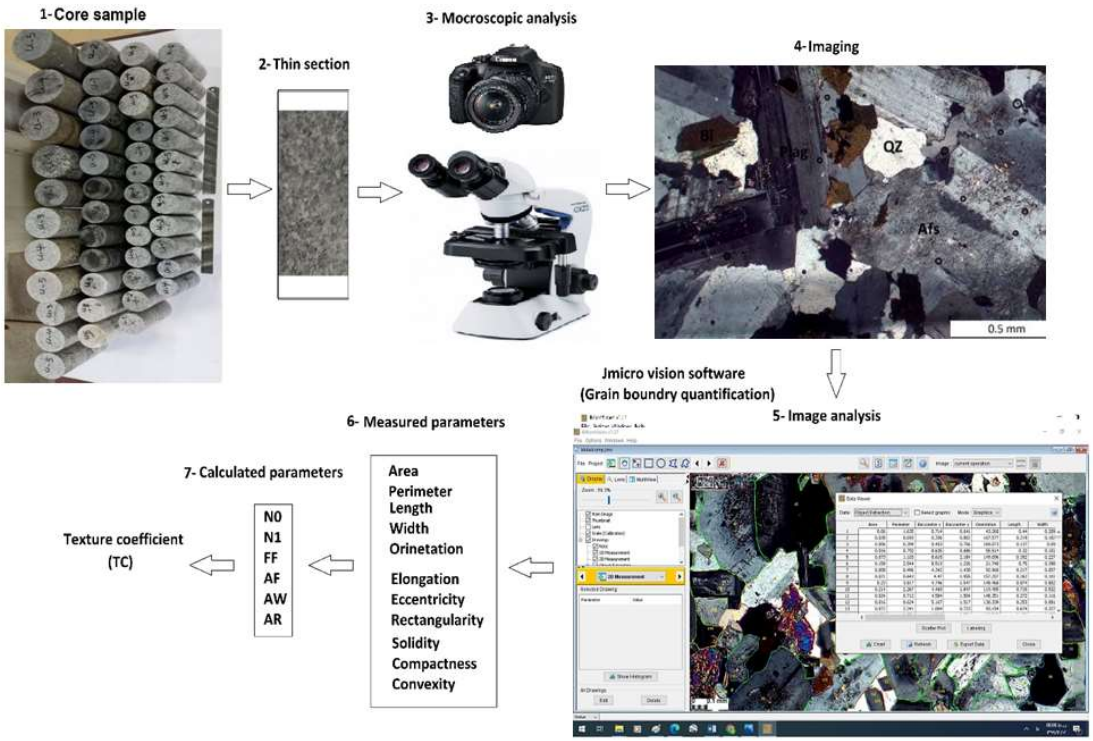

Figure 8. Workflow used in JMicroVision (v.1.27) for determining the texture coefficient (TC) from thin-section images

A common technique for analyzing rock texture involves the digital processing of images taken from thin sections (Prikryl, 2006; Akesson et al., 2003; Tandon and Gupta, 2013; Undul, 2016). A standard procedure for this analysis is the Texture Coefficient (TC) method, originally developed by Howarth and Rowlands (1987). This practical TC approach has been widely adopted in research to predict various geotechnical properties and to classify different rock types (Figure 7) (e.g., Ersoy and Waller, 1995; Azzoni et al., 1996; Alber and Kahraman, 2009).

Rock texture is characterized by several factors, including the geometrical properties of its grains, their interlocking index, and their packing density. Quantifiable grain shape and size attributes are derived from digital measurements of perimeter, area, maximum and minimum Feret's diameters, eccentricity, elongation, rectangularity, solidity, compactness, and convexity. These measurements are used to calculate specific coefficients, such as the Aspect Ratio (AR; Eq. (1)) and Form Factor (FF; Eq. (2)). A perfect circle or regular polygon has an AR value of 1, while all other shapes yield a value greater than 1. Conversely, the FF value decreases as a grain's elongation and surface roughness increase.

The packing density, which reflects the proportion of grains to the surrounding matrix, is determined by the Area Weighting (AW; Eq. (3)) parameter. This ratio highlights the influence of pores, matrix material, and weathered minerals within the analyzed area. An AW value of 1 indicates a sample devoid of pores, whereas a value below 1 signifies the presence of a matrix or weathered minerals (Howarth and Rowlands, 1987).

Furthermore, the angular orientation of grains is defined by the Angle Factor (AF), a metric calculated exclusively for elongated grains (those with AR > 2). The AF is computed using a class-weighted system based on the critical angular differences between these elongated grains (Eq. (4)). These angular differences are categorized into nine classes (0–10°, 11–20°, ..., 81–90°), each assigned a weighting factor from 1 to 9, respectively.

$$AR = \frac{L}{W} \tag{1}$$

$$FF = \frac{4\pi A}{P^2} \tag{2}$$

$$AW = \frac{\sum \text{Grain areas within the reference area boundary}}{\text{Area boundary by the reference area}} \tag{3}$$

$$AF = \sum_{i=1}^{9} \frac{Xi}{\frac{n(n-1)}{2}} \times i \tag{4}$$

The variable *n* in this equation denotes the total quantity of elongated grains, while *xi* represents the frequency of angular differences found within each specific class. Furthermore, the physical characteristics of grains–namely their length (L), width (W), area (A), and perimeter (P)–serve as fundamental metrics for defining their shape and size. These primary measurements are subsequently used to calculate descriptive coefficients, including the aspect ratio (AR) and form factor (FF).

The parameters AR, FF, AW, and AF provide a quantitative description of rock texture. Elevated values of these indices, which denote a more interlocked and dense granular structure, are known to positively influence the rock's geotechnical characteristics. This relationship is formally quantified using the Texture Coefficient (TC), as defined by Equation (5) *(Howarth and Rowlands, 1987).*

$$TC = \left[\left(\frac{N_0}{N_0+N_1}\right) \times \left(\frac{1}{FF_0}\right) + \left(\frac{N_0}{N_0+N_1}\right) \times (AR_1) \times (AF_1)\right] \times AW \tag{5}$$

In this model, the values $\mathbf{N_0}$ and $\mathbf{N_1}$ represent the particle counts for grains with an Aspect Ratio (AR) below and above the established categorization threshold of 2, respectively. The terms FF_0 and AR_1 correspond to the arithmetic means of the Form Factor (FF) and Aspect

Ratio (AR) for their respective discriminated groups. Furthermore, the parameter AF_1 is a normalized value derived by dividing the original Angle Factor (AF) by 5 (i.e., $AF_1 = AF/5$).

The index g, calculated using Equation (6), represents the arithmetic mean of the rock grains' perimeter ratio. A higher value for this index signifies a greater degree of complexity and irregularity in the grains' boundary shapes (Prikryl, 2006).

$$g = \frac{1}{n} * \sum \frac{Lpi}{\sqrt{Ai}} \quad (6)$$

The parameter H quantifies variations in grain size distribution. These variations influence the rock's micro-cracking behavior and, consequently, its overall strength.

$$H = \sqrt{\sum_{i=1}^{m} \left(\frac{ri}{Ra} - 1\right)^2} \quad (7)$$

$$Ra = \sum_{i=1}^{m} wi * ri \quad (8)$$

In this context, the terms are defined as follows: ri is the mean grain size, Ra is the average grain size for various component minerals, Wi is the volume fraction, and m represents the mineral type (Peng et al., 2017).

To analyze rock texture, thin-section images in JPG format were prepared and examined using JMicroVision V.1.27 software, a tool specifically designed for high-resolution petrographic image analysis that supports both automatic and manual quantification (Roduit, 2009). For each sample, 360 digital photomicrographs were systematically captured to cover the entire thin-section surface under three distinct lighting conditions: plane-polarized light (PPL), cross-polarized light (XPL), and polarized light with a 45° stage rotation.

Following image acquisition, distortions and skewness were corrected during preprocessing. The individual images were then merged using Adobe Photoshop to create comprehensive mosaic image layers. Grain boundaries were traced by manually outlining each grain along adjacent interfaces, using the three overlaid mosaic layers as a reference. Simultaneously, mineral grains were identified and documented based on their optical properties exhibited across the image layers.

Key grain boundary parameters–including perimeter, area, size, maximum and minimum Feret's diameters, eccentricity, elongation, rectangularity, solidity, compactness, and convexity–were calibrated, digitized, and automatically computed. Derived coefficients such as AR, FF, AW, and AF were estimated using Equations (1) to (4). Finally, the Texture Coefficient (TC) was determined via Equation (5). Mean values for fundamental shape and size descriptors, fabric characteristics, and mineralogical indexes are summarized in Table 5.

Physical tests

The physical properties of the rock samples, including porosity (n, %), saturated density (ρ_{sat} gr/cm³), and dry density (ρ_d gr/cm³), were determined following the testing standards outlined by the International Society for Rock Mechanics (Duzgoren et. al. 2002). Porosity and dry density measurements were conducted in triplicate for each sample to ensure precision, with mean values are illustrated in Figures 9 and 10. The porosity of the tested granitic rocks ranged from 0.47 to 1.45%, while densities varied between 2.61 and 2.89 gr/cm³, reflecting the lithological diversity of the samples. According to the classification proposed by Anon (1977), the samples exhibit high to very high density, while their porosity falls within the low to very low range. The average density values for Monzo-granite, Quartz Syenite, Syenogranite, Quartz Monzonite, and Granodiorite were 2.75, 2.78, 2.66, 2.76, and 2.68 gr/cm³, respectively. The corresponding mean porosity values were 0.88%, 0.92%, 0.85%, 0.76%, and 1.02%. These results show that all rock types display relatively high density and very low porosity, consistent with the characteristics of compact, crystalline igneous rocks.

Table 5. The petrographic features of the studied rocks

Sample Number	UTM-X	UTM-Y	Petrographic Name	Area (mm^2)	Size (mm)	TC	H
KG-1	530604	4067944	Monzo-granite	0.1	0.28	1.76	2.37
KG-2	531816	4069809	Quartz Syenite	0.15	0.34	1.77	2.09
KG-3	533159	4071946	Syenogranite	0.07	0.13	1.72	1.88
KG-4	535746	4075968	Quartz monzonite	0.3	0.56	1.51	1.69
KG-5	535382	4075459	Quartz Syenite	0.47	0.68	0.99	0.95
KG-6	531237	4068875	Quartz Syenite	0.04	0.15	2.03	2.2
KG-7	531510	4069285	Quartz Syenite	0.04	0.2	1.91	1.9
KG-8	533636.18	4072902.5	Quartz Syenite	0.2	0.25	1.4	1.36
KG-9	534220	4073526	Syenogranite	0.18	0.22	1.54	1.44
KG-10	540005	4082740	Syenogranite	0.12	0.3	1.82	2.37
KG-11	530883	4068337	Syenogranite	0.2	0.42	1.78	2
KG-12	531051	4068595	Syenogranite	0.17	0.29	1.71	1.7
KG-13	539085	4081327	Syenogranite	0.13	0.2	1.8	1.66
KG-14	535321	4075142	Granodiorite	0.08	0.22	1.52	1.55
KG-15	541738.65	4083769	Syenogranite	0.12	0.38	1.25	1.4
KG-16	539516	4082029	Syenogranite	0.09	0.27	1.5	1.5
KG-17	530440	4067795	Monzo-granite	0.011	0.05	1.87	1.95
KG-18	530061	4067384	Monzo-granite	0.49	0.68	0.93	1.36
KG-19	540544.46	4082926.8	Monzo-granite	0.24	0.4	1.56	1.61
KG-20	540924.95	4082926.8	Monzo-granite	0.47	0.68	1.57	1.68
KG-21	538735	4080749	Monzo-granite	0.33	0.51	1.67	1.81
MTG-1	538203	4079902	Monzo-granite	0.09	0.2	1.9	1.83
MTG-2	536969	4077931	Monzo-granite	0.07	0.25	1.84	1.88
MTG-3	536218	4076728	Monzo-granite	0.08	0.26	1.95	1.85
MTG-4	534776	4074474	Monzo-granite	0.10	0.3	1.92	1.86
MTG-5	536602	4077375	Monzo-granite	0.13	0.32	1.78	1.82
MTG-6	535914	4076264	Monzo-granite	0.11	0.23	1.81	1.83
MTG-7	531534	4067543	Monzo-granite	0.19	0.25	1.77	1.77
MTG-8	532113	4070233	Monzo-granite	0.20	0.27	1.78	1.74
MTG-9	533536	4072477	Monzo-granite	0.20	0.3	1.72	1.75
MTG-10	538471	4080379	Monzo-granite	0.14	0.25	1.83	1.78
MTG-11	531108	4068213	Monzo-granite	0.13	0.24	1.84	1.83
MTG-12	537747	4079199	Monzo-granite	0.06	0.25	1.93	1.90
MTG-13	537315	4078564	Monzo-granite	0.10	0.3	1.85	1.85
MTG-14	532809	4071424	Monzo-granite	0.20	0.32	1.78	1.76
MTG-15	532598	4071027	Monzo-granite	0.18	0.26	1.88	1.84
MTG-16	532286	4070556	Monzo-granite	0.22	0.35	1.82	1.76
MTG-17	540552	4083651	Monzo-granite	0.17	0.27	1.92	1.87
MTG-18	540913	4084191	Monzo-granite	0.10	0.15	2.1	2.08
MTG-19	541263	4084756	Monzo-granite	0.20	0.1	2.2	2.05
MTG-20	541472	4085112	Monzo-granite	0.18	0.12	2.12	2.06

* Size: Equivalent circular diameter; Area: Number of pixels in the object; TC: Texture coefficient;
** KG, MTG: Sample identifiers (e.g., KG-1, MTG-1) listed in Table 2 are laboratory codes used for data processing and model development.

Mechanical tests

The mechanical properties of the rock samples were characterized through some key tests namely rock strength (UCS, E, BTS, and IS_{50}, MPa), wave velocity (V_P, V_S, m/s), Schmitt

hammer Index, and Punch strength index (P_d, MPa). They were conducted in accordance with ISRM standards. Each test was repeated three times per sample to ensure reliability, with mean values are illustrated in figures 11 to 18.

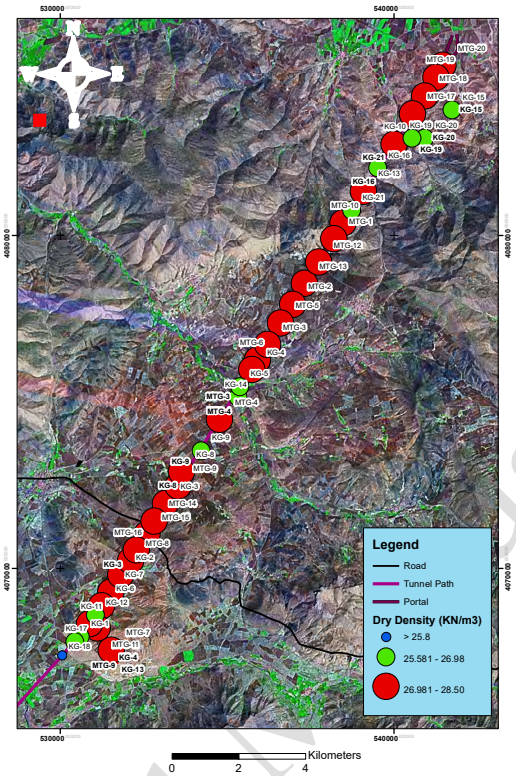

Figure 9. The density distribution classified across the study area

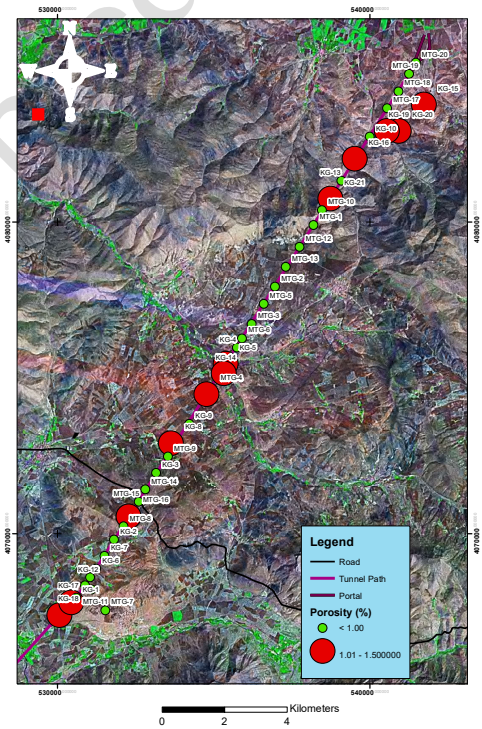

Figure 10. The porosity distribution classified across the study area

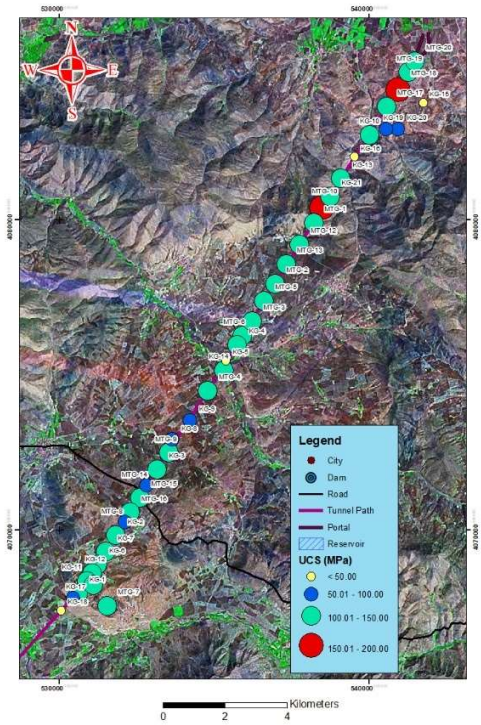

Figure 11. The UCS distribution classified across the study area

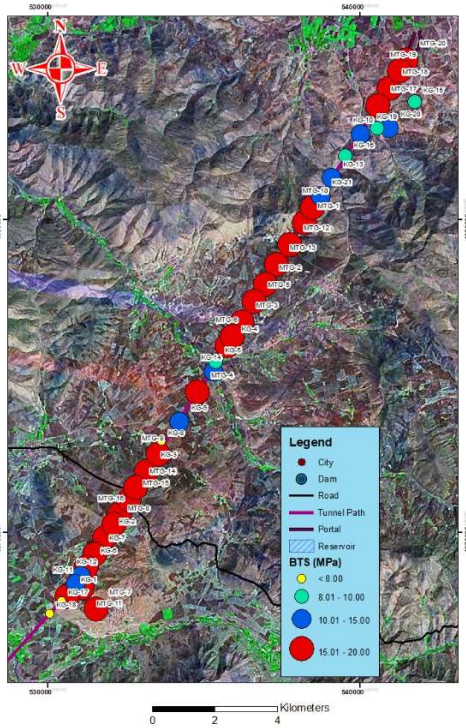

Figure 12. The BTS distribution classified across the study area

The average of Mechanical properties of Granitic type rocks, including the results of the UCS test, IS50 test, and E, were between 35.73 and 182.5 MPa, 2.05 and 9.40 MPa, and 10.64 and 59.03, respectively. According to the ISRM classification (2007), the UCS values were low to high. Based on the Bieniawski classification (1975), the IS50 values were high to very high. According to the IAEG (1979), the elastic modulus values were moderate to high.

The mean UCS values for Syenogranite, Monzo-granite, Quartz Syenite, and Quartz Monzonite were 92.40, 114.98, 105.55, and 119.00 MPa, respectively. The corresponding average elastic modulus (E) values were 36.11, 40.00, 32.09, and 49.23 GPa. Based on the modulus ratio (MR) classification proposed by Deer and Miller (1966), the calculated MR values place these rocks within the M-class category.

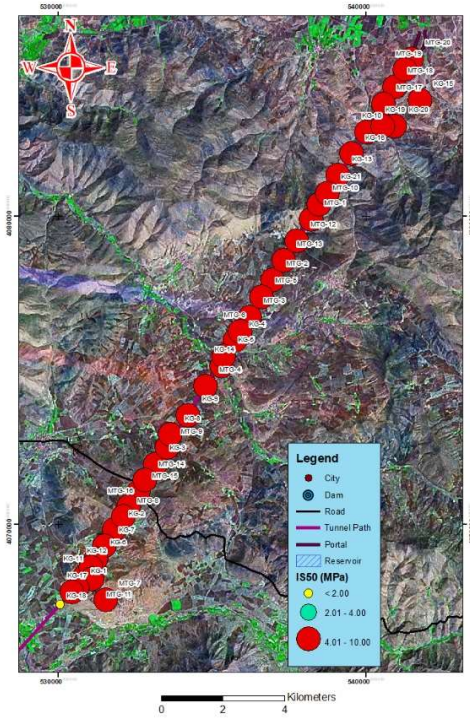

Figure 13. The IS_{50} distribution classified across the study area

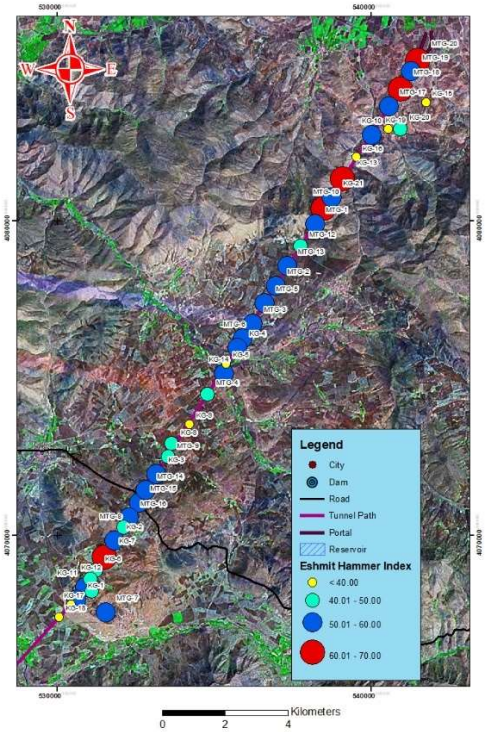

Figure 14. The SH distribution classified across the study area

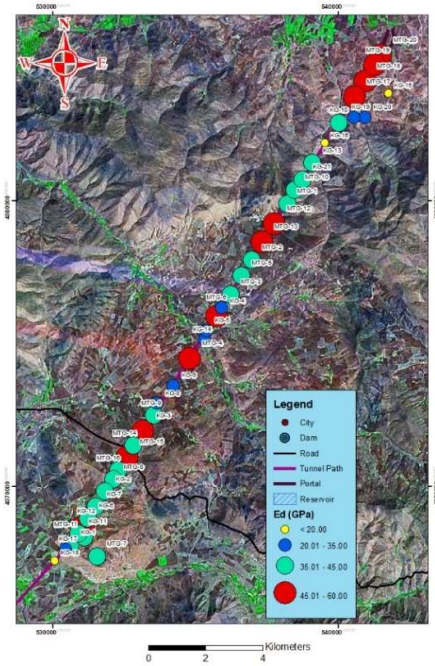

Figure 15. The Elastic modulus distribution classified across the study area

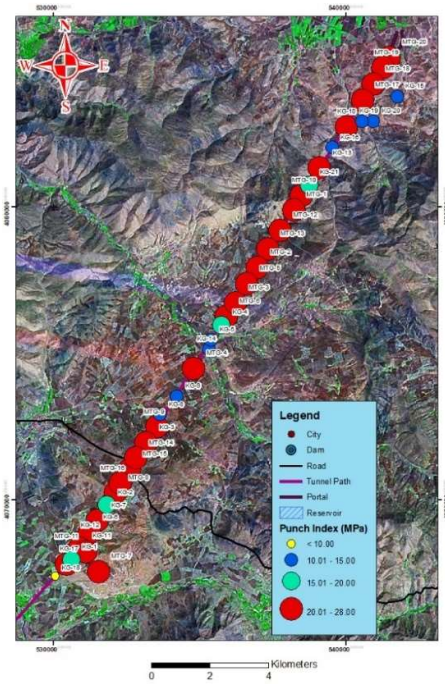

Figure 16. The Punch Strength Index distribution classified across the study area

The mean IS_{50} values for Syenogranite, Monzo-granite, Quartz Syenite, and Quartz Monzonite were 6.48, 6.79,6.95, and 6.97 MPa, respectively. Based on the Bieniawski classification (1975), the mean IS_{50} values were high.

The mean P-wave (V_p) and S-wave (V_s) velocities of the studied granitic rocks were also measured to evaluate their elastic and mechanical behavior. The average Vp values for Syenogranite, Monzo-granite, Quartz Syenite, and Quartz Monzonite were 56.36, 58.12, 57.20, and 56.69 km/s, respectively, while the corresponding Vs values were 29.41, 30.03, 29.97, and 29.49 km/s. Based on standard classifications for crystalline rocks (Telford et al., 1990; Wang,

2000), these Vp values fall within the high-velocity range, indicating that the samples are dense and compact. The Vs values, which range from moderate to high, reflect substantial shear strength and rigidity of the rocks. Taken together, the high P-wave and moderate-to-high S-wave velocities confirm that these granitic rock types are mechanically competent and typical of felsic, plutonic igneous rocks. These results are consistent with the previously observed high density, low porosity, and strong mechanical properties, suggesting that quartz and feldspar content significantly influence the elastic and seismic behavior of the samples.

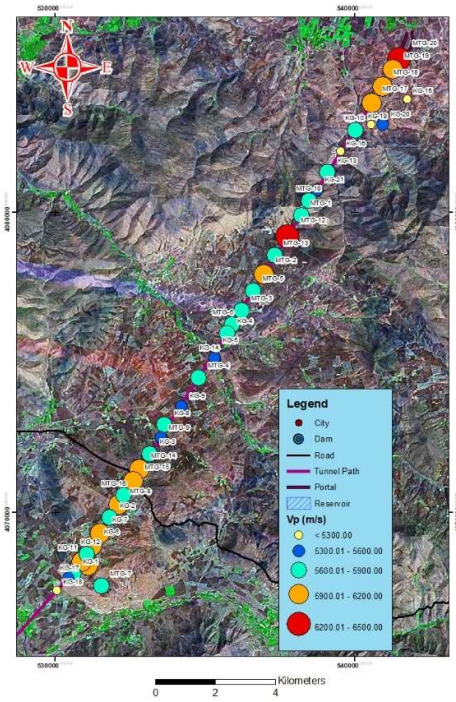

Figure 17. The V_p distribution classified across the study area

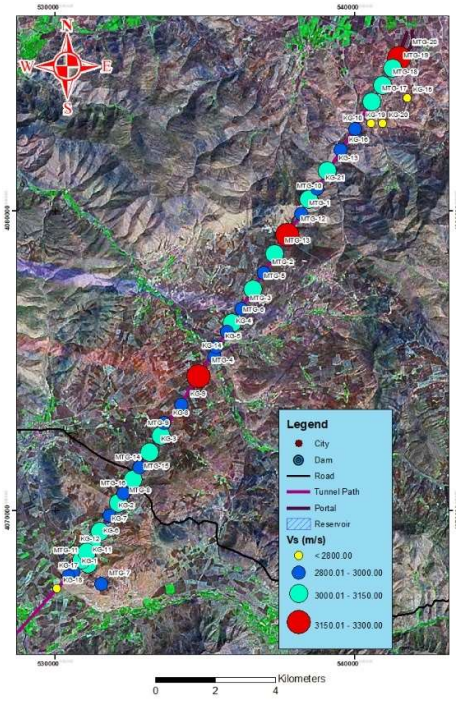

Figure 18. The V_s distribution classified across the study area

The tensile properties of the studied rock types were evaluated using the Brazilian Tensile Strength (BTS) and Punch Strength Index (P_d) tests. The mean BTS values for Syenogranite, Monzo-granite, Quartz Syenite, and Quartz Monzonite were 12.68, 21.32, 12.98, and 16.52 MPa, respectively. Similarly, the corresponding average punch strength values were 18.89, 15.64, 17.58, and 19.84 MPa. According to the ISRM Suggested Methods (1978, 1985), these values are consistent with the tensile and punch strength ranges typically observed in compact crystalline rocks. Variations among the samples can be attributed to differences in mineralogical composition, microfracture density, and grain-boundary characteristics, all of which are known to influence the tensile response of granitic rocks (Bieniawski, 1975; Hoek & Brown, 1980).

Variations in quartz and feldspar contents appear to influence the physical and mechanical behavior of the analyzed samples. An increase in quartz content generally enhances the overall strength of granitic rocks, whereas higher proportions of feldspar tend to reduce their mechanical strength, a trend consistent with the findings of Tugrul and Zarif (1999).

Abrasion test

Rock abrasivity is a critical factor influencing tool wear in tunnel boring machines (TBMs) and mining excavation. The Cerchar abrasivity index (CAI) test has become the benchmark for assessing abrasivity due to its rapid, cost-effective and standardized procedure. In this study, the CAI was determined using a hardened 54–56 HRC steel stylus (Afnor, 2000, Cerchar, 1986) under a static load of 70 N, which was drawn across the smooth surface of 100 mm diameter core samples at 1 mm/s to produce 10-mm-long scratches (Figure 19). Following ISRM guidelines, five tests per sample were conducted, with at least three scratches per test. Post-test, stylus tip wear was quantified using a reflective light microscope integrated with scaling software. The resulting CAI values, averaged across replicates, ranged from 1.3 to 3.95, classifying the samples as low to very high abrasiveness according CAI abrasivity classification in Table 6 (Albert et.al. ,2014). The spatial distribution of CAI values across the studied tunnel is illustrated in Figure 20, while representative scratched surfaces and worn stylus tips are depicted in Figure 19.

The mean Cerchar Abrasivity Index (CAI) values for Syenogranite, Monzo-granite, Quartz Syenite, and Quartz Monzonite were 2.69, 2.89, 2.40, and 2.54, respectively. According to the Cerchar abrasivity classification (Plinninger, 2010; Cerchar, 1972), CAI values between 2 and 3 indicate moderately abrasive rock materials. All four granitic rock types fall within this category, reflecting the presence of hard minerals such as quartz and feldspar. Among the samples, Monzo-granite exhibits the highest abrasivity, followed closely by Syenogranite, suggesting a slightly greater potential for tool wear during drilling or cutting operations. Quartz Syenite and Quartz Monzonite show somewhat lower CAI values but still remain within the moderate abrasivity range. These differences can be attributed to variations in quartz content, grain interlocking, and micro-textural properties, which are known to influence the wear behavior of crystalline rocks.

Table 6. CAI abrasivity classification (Alber,et.al., 2014)

Classification	Mean CAI range
Extremely low	0.1-0.4
Very Low	0.5-0.9
Low	1.0-1.9
Medium	2.0-2.9
High	3.0-3.9
Very high	4.0-4.9
Extremely high	> 5.0

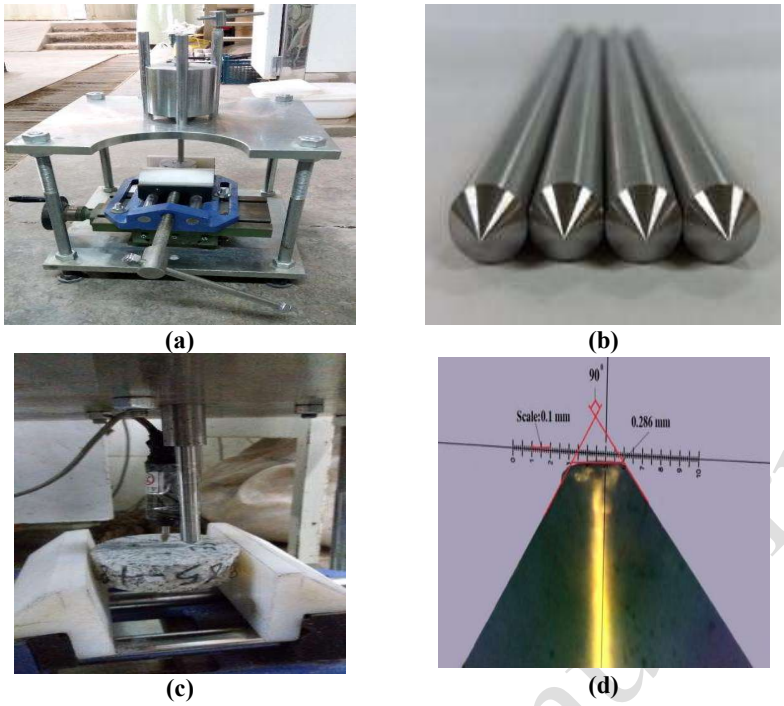

Figure. 19. Cerchar testing method (a) Cerchar testing apparatus, (b) Cerchar pins used in this research, (c) Scratches made on the sample by pins in the Cerchar test, and (d) Imaging system and study of pin tip shape after tests

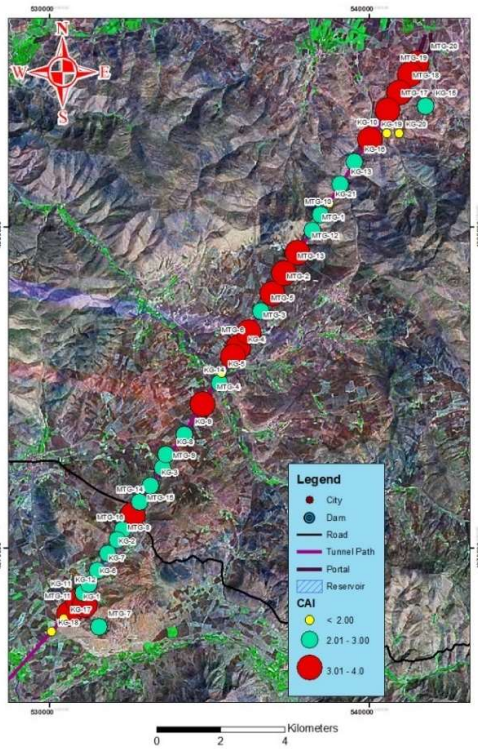

Figure 20. The CAI distribution classified across the study area

Drilling rate index

The Drilling Rate Index (DRI) quantifies the relative ease or difficulty of drilling through rock formations. This testing methodology was originally developed at the Engineering Geology

Laboratory of the Norwegian Institute of Technology (NTH) during the 1960s. Notably, NTH has since been reorganized and is now known as the Norwegian University of Science and Technology (NTNU) (Nilsen, 2003). The DRI is derived from two constituent tests: a brittleness test (S_{20}) and the Sievers' J-value (S_J). All DRI testing procedures referenced in this study were conducted in accordance with the standards established by Dahl (2003).

The S_J miniature drill test

The Sievers' J-value test serves as a means to evaluate key rock properties, including cutter life, surface hardness, and resistance to indentation penetration (Bruland, 2000). This value is determined by calculating the average depth of the drill hole—measured in tenths of a millimeter—after 200 revolutions with an 8.5-mm miniature drill bit. To ensure accuracy and reproducibility, the test is repeated between four and eight times per rock sample. The standard procedure requires the use of a pre-cut surface on the sample, as specified by Dahl (2003). A visual representation of the Sievers' J test apparatus can be seen in Figure 21a.

The mean Sievers' J-values (S_J) for Syenogranite, Monzo-granite, Quartz Syenite, and Quartz Monzonite were 7.31, 10.14, 6.33, and 5.44 mm/10, respectively. Based on standard S_J-value interpretations (Plinninger, 2010), values between 5 and 10 mm/10 indicate moderate to high brittleness. Among the tested rock types, Monzo-granite exhibits the highest S_J-value, suggesting the greatest brittleness and the highest likelihood of chipping or fragmentation during mechanical excavation. Syenogranite also shows moderately high brittleness, whereas Quartz Syenite and Quartz Monzonite display slightly lower S_J-values, indicating comparatively less brittle but still moderately breakable behavior. These variations in S_J-values are likely influenced by differences in mineral proportions, grain-boundary characteristics, and microfracture distribution, all of which affect the fragmentation response of crystalline rocks

The brittleness test

The brittleness test measures a rock's capacity to withstand repeated impact crushing and the energy consumed in the fracturing process (Bruland, 1999; Wilfing, 2016). For this procedure, a standardized sample mass of 500 g is prepared, comprising rock chips with a density of 2.65 g/cm³ that pass through a 16-mm sieve but are retained on an 11.2-mm mesh. The brittleness value, denoted as S_{20}, is defined as the percentage of material that passes the 11.2-mm sieve after the aggregate has been subjected to 20 impacts from a 14-kg hammer. This value is derived as the average of three to five individual test repetitions (Dahl, 2003). The apparatus used for the brittleness test is illustrated in Figure 21b.

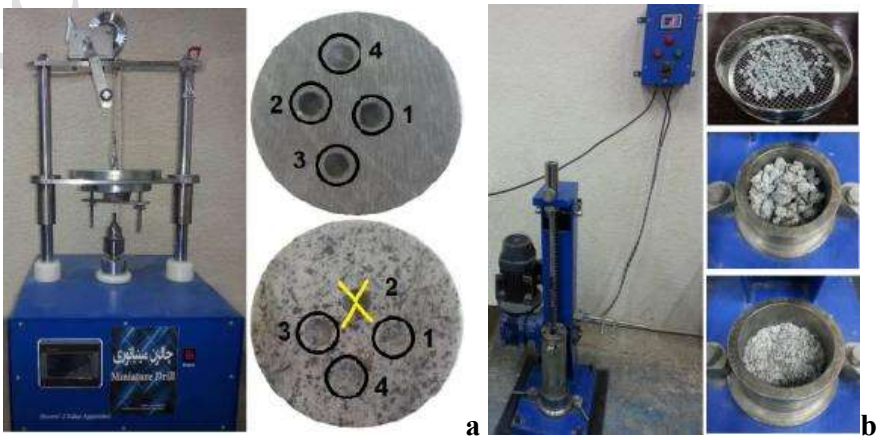

a b

Figure 21. a) Sievers' J-miniature drill test apparatus. b) Brittleness test apparatus

The mean brittleness values (S_{20}) for Syenogranite, Monzo-granite, Quartz Syenite, and Quartz Monzonite were 47.05, 40.98, 41.90, and 53.15, respectively. According to commonly applied brittleness classifications (Hucka & Das, 1974; Kahraman, 2002, Dahl, 2003), S_{20} values greater than 40 indicate moderate to high brittleness. Among the studied rock types, Quartz Monzonite displays the highest brittleness, followed by Syenogranite, suggesting a greater tendency for fragmentation during cutting or excavation processes. Monzo-granite and Quartz Syenite exhibit slightly lower S_{20} values but remain within the moderately brittle category. These variations in brittleness reflect differences in quartz content, mineral interlocking, and microfracture density, which strongly influence how crystalline rocks respond to mechanical loading. The Drilling Rate Index (DRI) is subsequently calculated using both the brittleness value (S_{20}) and the Sievers' J-value (S_J). The relationship between these parameters is presented graphically in the DRI diagram (Figure 22), while the corresponding classification system for DRI values is provided in Table 7 (Dahl, 2003).S_J and S_{20} tests were performed according to the NTNU/SINTEF standard (Dahl, 2003).

Drillability properties, including the results of the S_J, S_{20}, and DRI values, were between 2.08 and 52.0, 24.64 and 60.0, and 20.5 and 70.00, respectively. According to the DRI classification (Dahl, 2003) (Table 7), the DRI values were Extremely low to very high. The spatial distribution of S_{20}, S_J, and DRI values across the studied tunnel are illustrated in Figures 23 to 25.

The mean Drilling Rate Index (DRI) values for Syenogranite, Monzo-granite, Quartz Syenite, and Quartz Monzonite were 44.86, 37.88, 40.00, and 43.00, respectively. According to the NTNU–SINTEF drilling performance classification (Bruland, 1998; Bruland, 2000), DRI values between 30 and 55 indicate moderately drillable to fairly drillable rock conditions. Based on this range, all four rock types fall into the moderately drillable category, with Syenogranite and Quartz Monzonite showing slightly higher DRI values, implying somewhat easier penetration during mechanical drilling.

Table 7. Classification of DRI (Dahl, 2003)

Classification	Mean DRI range
Extremely low	<25
Very Low	26-32
Low	33-42
Medium	43-57
High	58-69
Very high	70-82
Extremely high	> 83

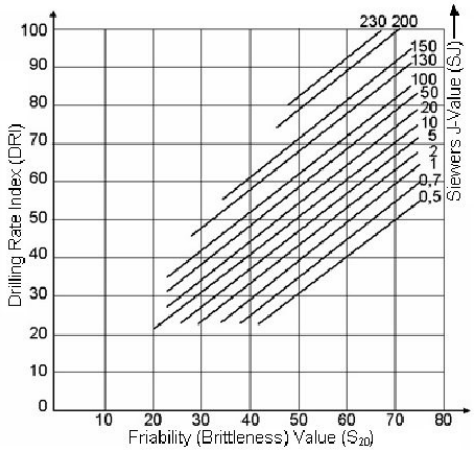

Figure 22. DRI diagram for calculation of DRI (Dahl, 2003)

Monzo-granite records the lowest DRI value, suggesting marginally greater resistance to drilling, likely due to its higher quartz content and stronger interlocking texture. These variations in DRI are consistent with the observed differences in brittleness, abrasivity, and seismic velocities, all of which influence drillability in granitic rocks.

Rock hardness and abrasively indexes

The Drilling Rate Index (DRI) and Bit Wear Index (BWI) are both indirect indicators used to assess rock drillability. However, due to limitations in BWI's effectiveness for predicting drill bit longevity in drill and blast tunneling operations, the Vickers Hardness Number of Rock (VHNR) has been increasingly adopted as a more reliable alternative in contemporary predictive models (NTNU, 2009; Zare & Bruland, 2013). VHNR is additionally utilized to estimate the service life of button drill bits (NTNU, 2007).

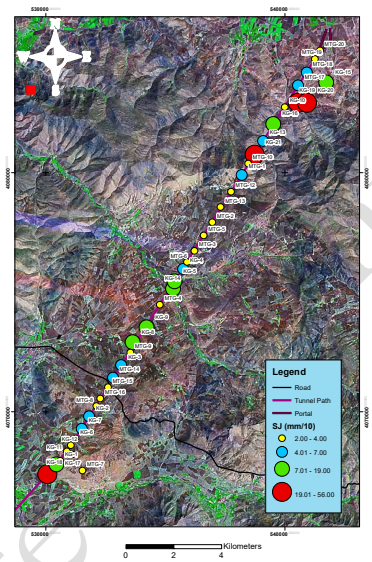

Figure 23. The S_J value distribution classified across the study area

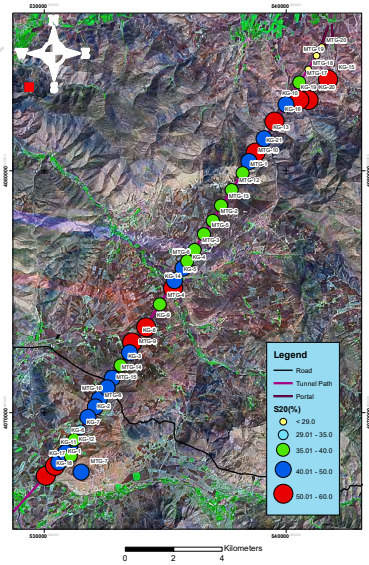

Figure 24. The S_{20} value distribution classified across the study area

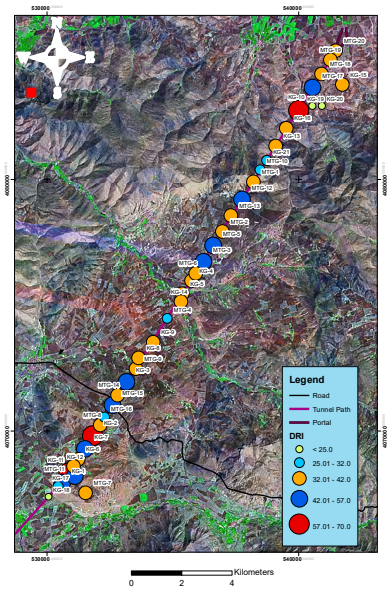

Figure 25. The DRI distribution classified across the study area

VHNR quantifies the composite hardness of the constituent minerals within a rock sample (Bruland, 1998). This metric is calculated by integrating the individual hardness values of each mineral present with their corresponding volumetric proportions in the rock. Consequently, VHNR provides a comprehensive measure that reflects both the mineralogical composition and the inherent hardness of the sample's minerals. The VHNR for each rock type was determined using Equation 9.

$$VHNR = \sum VHNRi \times (mineral(\%/100) \quad (9)$$

The Vickers Hardness Number of Rock (VHNR) is conceptually analogous to the Equivalent Quartz Content (EQC) index, an alternative measure of rock hardness employed by researchers such as Thuro (1997). Like VHNR, the EQC offers a methodology for assessing overall rock hardness and is computed using Equation 10.

$$\mathrm{EQC} = \sum_{i=1}^{n} \mathrm{Ai.\,Ri}(\%) \quad (10)$$

In this equation, Ai represents the percentage of each constituent mineral, Ri denotes the Rosiwal hardness, a value derived from the quartz content percentage, and *n* signifies the total number of distinct minerals present in the sample. Mineralogical composition was quantified through analysis conducted with a petrological microscope.

Subsequently, three distinct indexes of abrasiveness are introduced. Among these, the Abrasivity Index (ABI) serves as a metric for assessing rock abrasiveness. This composite metric is calculated as the product of two fundamental properties: The Vickers Hardness Number of Rock (VHNR) and the Uniaxial Compressive Strength (UCS), as defined in Equation 11 (Hassanpour et al., 2014).

$$\mathrm{ABI} = \mathrm{VHNR} \times 0.01\mathrm{UCS} \quad (11)$$

The Vickers Hardness Number of Rock (VHNR) is calculated as a weighted average of the Vickers hardness values of individual minerals within the rock's mineralogical composition, while UCS refers to the Uniaxial Compressive Strength, measured in megapascals (MPa).

To address limitations associated with earlier wear indices, the Rock Abrasivity Index (RAI) was developed. This index incorporates both Equivalent Quartz Content (EQC) and Uniaxial Compressive Strength (UCS) into its formulation, as shown in Equation 12 (Plinninger et .al., 2002).

$$\mathrm{RAI} = \mathrm{EQC} \times \mathrm{UCS} \quad (12)$$

Both the Abrasivity Index (ABI) and the Rock Abrasivity Index (RAI) serve as key metrics for evaluating rock strength and hardness. The drillability of rock, as characterized through the Sievers' J-value (S_J) and brittleness value (S_{20}) tests, has been well established in research. Specifically, the SJ test is recognized as a reliable method for determining rock hardness (Dahl et al., 2012). Conversely, the S_{20} test is widely regarded as an indirect measure of Uniaxial Compressive Strength (UCS), as supported by multiple studies (Yarali & Soyer, 2013; Hosseini et al., 2015; Iqbal & Abu Bakar, 2016; Yenice et al., 2018; Yenice, 2019). This relationship arises because a decrease in UCS generally leads to increased crushing and fragmentation during the S_{20} test.

Rock hardness and abrasively indexes, including the results of the EQC, VHNR, RAI, and ABI values, were between 2.22 and 64.78, 125.59 and 797.88,79.32 and 11822.35, and 44.87 and 1454.36, respectively. The Abrasivity Index (ABI) and the Rock Abrasivity Index (RAI), the Vickers Hardness Number of Rock (VHNR), and Equivalent Quartz Content (EQC) results with mean values are illustrated in Figures 26 to 29.

The mean Abrasivity Index (ABI) values for Syenogranite, Monzo-granite, Quartz Syenite, and Quartz Monzonite were 607, 838, 687, and 818, respectively. Similarly, the mean Rock Abrasivity Index (RAI) values for the same rock types were 4374, 5643, 4570, and 5619, respectively. According to standard abrasivity classifications (Rostami et al., 2014), ABI and RAI values in these ranges indicate high abrasivity, suggesting a strong potential for tool wear during mechanical excavation or cutting. Among the tested rocks, Monzo-granite and Quartz Monzonite exhibit the highest ABI and RAI values, implying greater abrasiveness compared to Syenogranite and Quartz Syenite.

The mean Vickers Hardness Number of Rock (VHNR) values for Syenogranite, Monzo-granite, Quartz Syenite, and Quartz Monzonite were 611, 699, 655, and 688 kg/mm², respectively, placing all samples within the high hardness category (Oliver & Pharr, 1992). The strong correlation between VHNR, ABI, and RAI reflects the influence of mineralogical composition—particularly quartz and feldspar content–on the abrasivity and hardness of granitic rocks. Monzo-granite consistently shows the highest hardness and abrasivity indices, aligning with its higher quartz content and more robust interlocking texture, while Syenogranite records the lowest values in comparison, although it still remains within the high-abrasivity range.

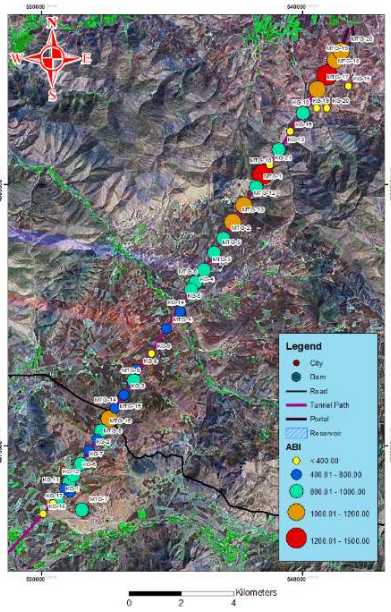

Figure 26. The ABI value distribution classified across the study area

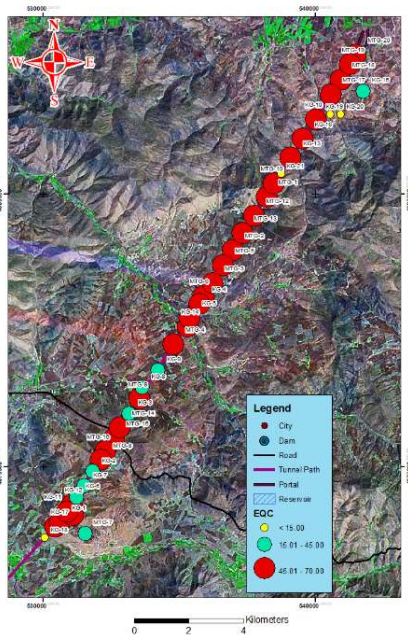

Figure 27. The EQC value distribution classified across the study area

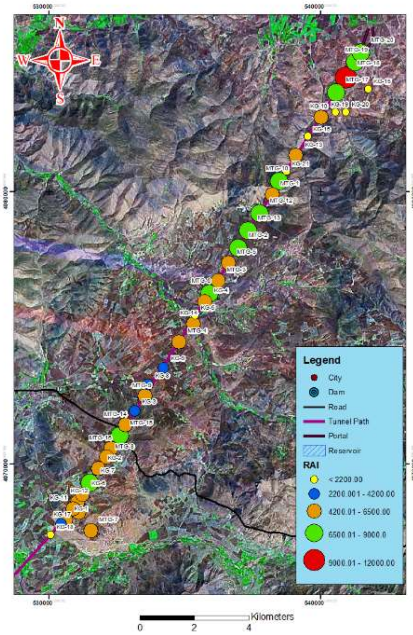

Figure 28. The RAI value distribution classified across the study area

Dataset collection

The main objective of this study was to evaluate the performance of proposed ensemble models in estimating DRI of rocks. A database comprising 41 rock units was initially compiled from experimental investigations, with a summary of the various input and output variables presented in Table 8 and their descriptive statistics in Table 9. The selection of input variables was guided by a thorough review of existing literature and aligned with domain-specific practices. They were chosen based on three key criteria: (1) established geomechanical relevance, as parameters like dry and saturated density, porosity, point load index, BTS and UCS are well-documented proxies for rock strength and tool-rock interaction, commonly used in DRI prediction studies

(Alber, 2008, Ko, et. al. 2016); (2) Fabric features and Abrasivity indices both of which significantly influence the DRI; and (3) practical field applicability, since all selected parameters are derived from standardized, low-cost tests (Price et.al. 2003), ensuring the model remains both scientifically sound and suitable for field use.

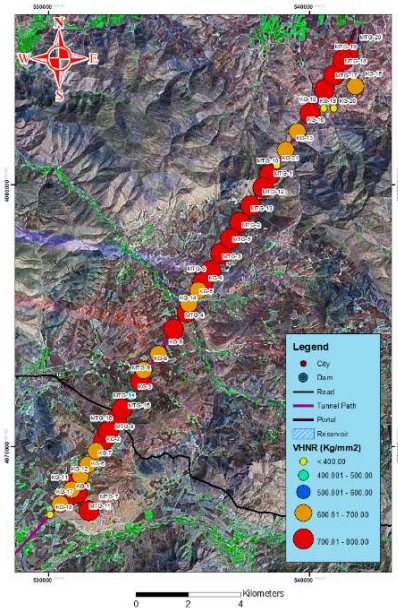

Figure 29. The VHNR value distribution classified across the study area

Table 8. Summary of input and output parameters used in study

Variables	Unit	Abbreviations
Input		
Area	(mm^2)	Area
Size	(mm)	
Texture Coefficient	-	TC
the difference of grain size distribution	-	H
Dry density	(gr/cm^3)	ρ_d
Saturated density	(gr/cm^3)	ρ_{sat}
Porosity	(%)	n
Compressional Wave Velocity	(m/s)	Vp
Shear Wave Velocity	(m/s)	Vs
Schmitt Hammer index	-	Sh
Point load index	(Mpa)	Is_{50}
Compressive Strength	(Mpa)	UCS
Elastic Modulus	(Gpa)	E
Tensile strength	(Mpa)	BTS
Punch strength index	(Mpa)	Pd
Cerchar abrasivity index	-	CAI
Equivalent Quartz Content	(%)	EQC
Vickers Hardness Number of Rock	(Kg/mm^2)	VHNR
Rock Abrasivity Index	-	RAI
Abrasivity Index	-	ABI
The Sievers' J-value	(mm/10)	S_J
brittleness value	(%)	S_{20}
Output		
Drilling Rate Index	-	DRI

Further, the frequency distribution of input and output variables are presented in Figures 30, 31, and Table 8. The histograms show the distribution of various geotechnical properties. Most parameters like ρ_d, ρ_{sat}, n, V_p, V_s, UCS, E, Is_{50}, pd, CAI, EQC, RAI, ABI, and S_{20} follow a near-normal distribution. Sh, BTS**,** AVI**,** Is_{50}, and VHNT are right-skewed, and S_J and DRI are left-skewed, indicating more frequent lower values. Overall, the data reflects consistent trends with slight variability across different properties. To address these variations, standard normalization was applied to all input features prior to training. This preprocessing step was integrated using a pipeline to ensure consistent and reproducible transformation across all machine learning models.

Table 9. Descriptive statistics of input and output parameters used in study

		Physical characteristics					Mechanical characteristics					
		ρ_d (gr/cm^3)	ρ_{sat} (gr/cm^3)	n (%)	V_p (m/s)	V_s (m/s)	Schmitt Hammer	UCS (MPa)	E (GPa)	Is_{50} (MPa)	BTS (MPa)	P_d (MPa)
N	Valid	41	41	41	41	41	41	41	41	41	41	41
	Missing	0	0	0	0	0	0	0	0	0	0	0
Mean		2.76	2.77	0.88	5756.97	2986.48	51.07	109.1749	38.33	6.7	14.65	20.18
Std. Error of Mean		0.10	0.09	0.04	45.73	23.15	1.58	5.12	1.68	0.27	0.59	0.74
Median		2.77	2.78	0.820	5834.00	2979.00	52.00	117.24	40.45	6.92	16.35	21.66
Mode		2.77	272.7829	0.62[a]	5049.00[a]	2649.00[a]	38.00	35.73[a]	46.27	4.20[a]	16.35	14.10
Std. Deviation		0.66	0.610	0.250	292.82	148.23	10.17	32.79	10.81	1.75	3.83	4.75
Variance		0.44	0.370	0.06	85744.07	21973.88	103.39	1075.46	116.941	3.06	14.65	22.62
Skewness		-0.40	-0.49	0.61	-0.44	-0.20	-0.8	-0.71	-0.68	-0.51	-0.87	-0.84
Std. Error of Skewness		0.37	0.37	0.37	0.37	0.37	0.37	0.37	0.37	0.37	0.37	0.37
Kurtosis		-0.07	0.32	-0.51	0.21	-0.39	.323	.563	.302	-.248	-.445	.013
Std. Error of Kurtosis		0.72	0.72	0.72	0.72	0.72	0.72	0.72	0.72	0.72	0.72	0.72
Range		0.28	0.28	0.98	1364.00	633.61	43.80	146.77	48.39	7.36	14.31	19.51
Minimum		2.61	2.62	0.47	5049.00	2649.00	26.00	35.73	10.64	2.04	5.30	8.20
Maximum		2.89	2.90	1.45	6413.00	3282.61	69.80	182.50	59.03	9.40	19.61	27.71

a. Multiple modes exist. The smallest value is shown

Cont.Table 9. Descriptive statistics of input and output parameters used in study

		Abrasivity indices					Drillability peoperties		
		CAI	EQC	VHNR	RAI	ABI	S_J	S_{20}	DRI
N	Valid	41	41	41	41	41	41	41	41
	Missing	0	0	0	0	0	0	0	0
Mean		2.81	46.46	687.95	5268.58	772.96	9.06	42.66	39.70
Std. Error of Mean		0.09	2.245	22.67	378.56	47.22	1.90	1.28	1.744
Median		2.86	49.33	749.78	5778.99	841.64	4.00	41.82	37.00
Mode		3.25	2.22[a]	125.59[a]	79.32[a]	44.87[a]	4.50	53.00	37.00
Std. Deviation		0.59	14.38	145.17	2423.98	302.38	12.16	8.172	11.16
Variance		0.35	206.66	21073.64	5875657.71	91432.46	147.79	66.78	124.66
Skewness		-0.54	-1.87	-2.26	-.213	-0.49	2.49	.22	0.750
Std. Error of Skewness		0.37	0.37	0.37	0.37	0.37	0.37	0.37	0.37
Kurtosis		.075	3.369	5.458	.563	.078	5.321	-.020	.197
Std. Error of Kurtosis		0.72	0.72	0.72	0.72	0.72	0.72	0.72	0.72
Range		2.65	62.56	672.29	11743.03	1409.49	49.92	35.36	49.50
Minimum		1.30	2.22	125.59	79.32	44.87	2.08	24.64	20.50
Maximum		3.95	64.78	797.88	11822.35	1454.36	52.00	60.00	70.00

a. Multiple modes exist. The smallest value is shown

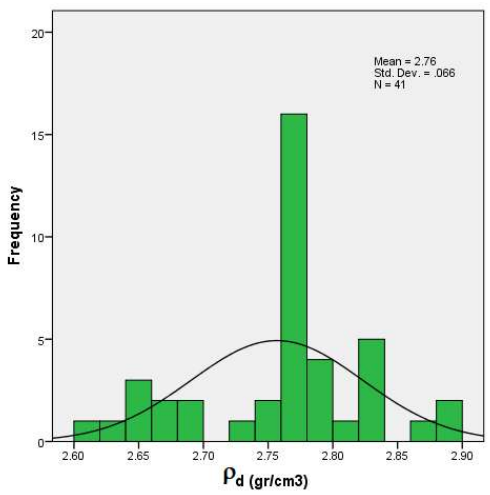
Mean = 2.76
Std. Dev. = .066
N = 41
Frequency
ρd (gr/cm3)

(a)

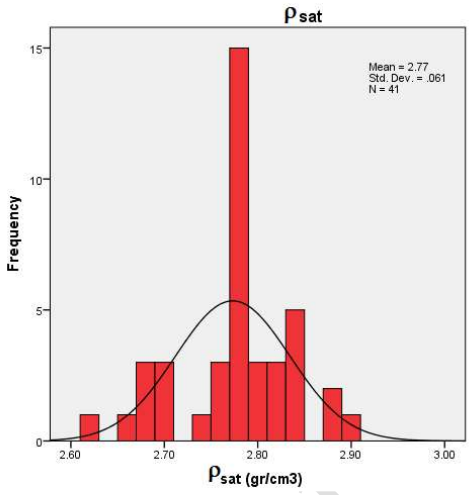
ρsat
Mean = 2.77
Std. Dev. = .061
N = 41
Frequency
ρsat (gr/cm3)

(b)

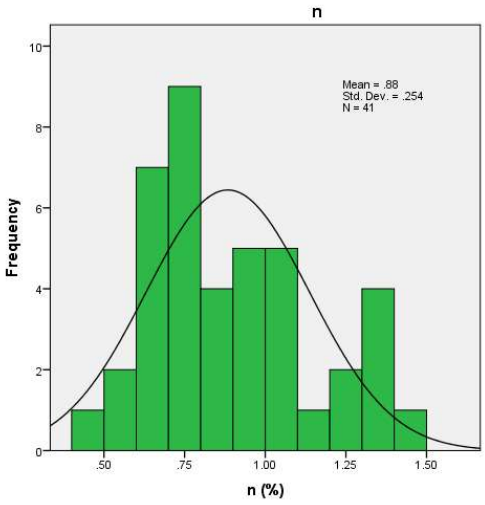
n
Mean = .88
Std. Dev. = .254
N = 41
Frequency
n (%)

(c)

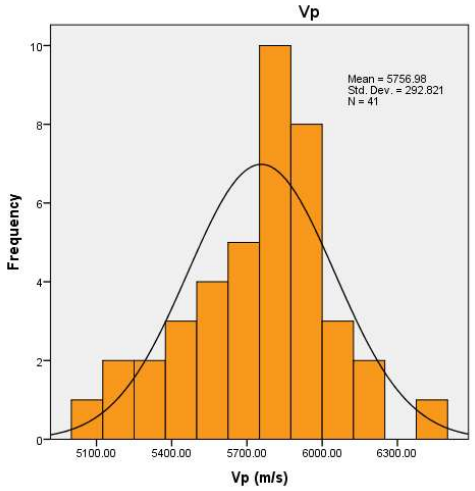
Vp
Mean = 5756.98
Std. Dev. = 292.821
N = 41
Frequency
Vp (m/s)

(d)

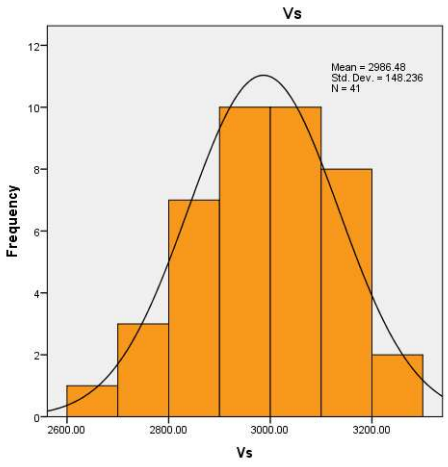
Vs
Mean = 2986.48
Std. Dev. = 148.236
N = 41
Frequency
Vs

(e)

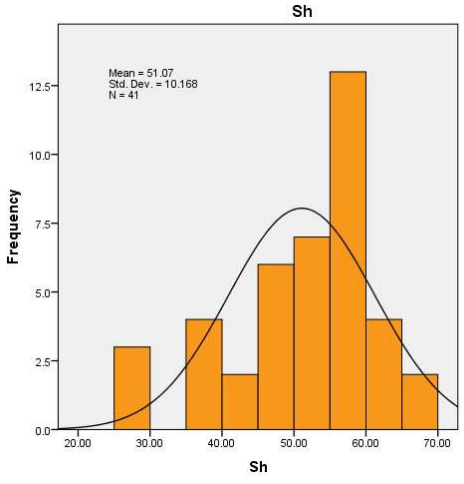
Sh
Mean = 51.07
Std. Dev. = 10.168
N = 41
Frequency
Sh

(f)

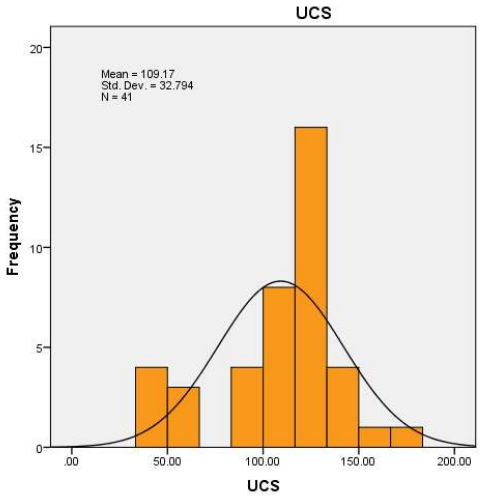
UCS
Mean = 109.17
Std. Dev. = 32.794
N = 41
Frequency
UCS

(g)

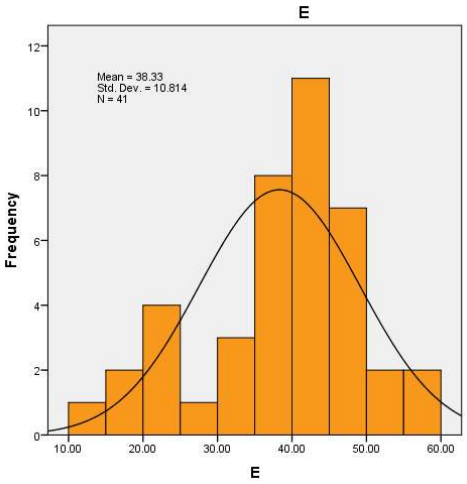
E
Mean = 38.33
Std. Dev. = 10.814
N = 41
Frequency
E

(h)

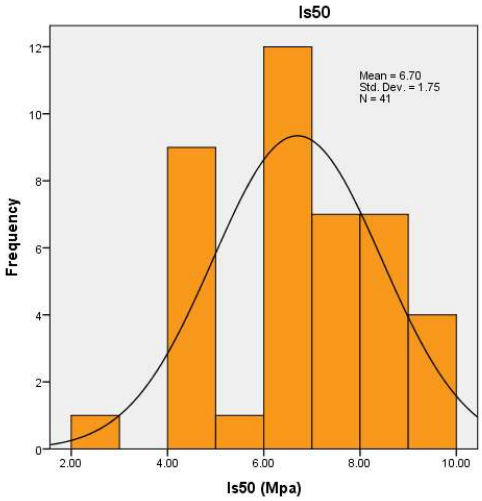
Is50
Mean = 6.70
Std. Dev. = 1.75
N = 41
Frequency
Is50 (Mpa)

(i)

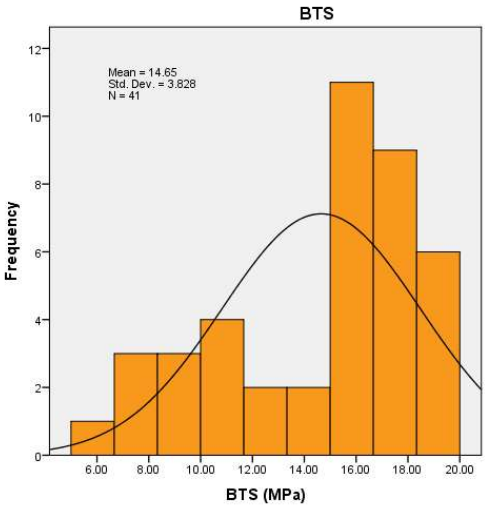
BTS
Mean = 14.65
Std. Dev. = 3.828
N = 41
Frequency
BTS (MPa)

(j)

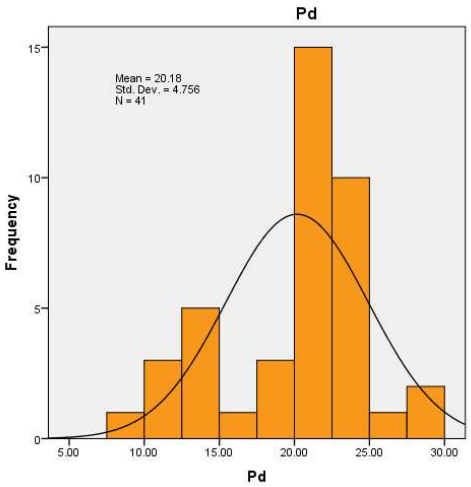
Pd
Mean = 20.18
Std. Dev. = 4.756
N = 41
Frequency
Pd

(k)

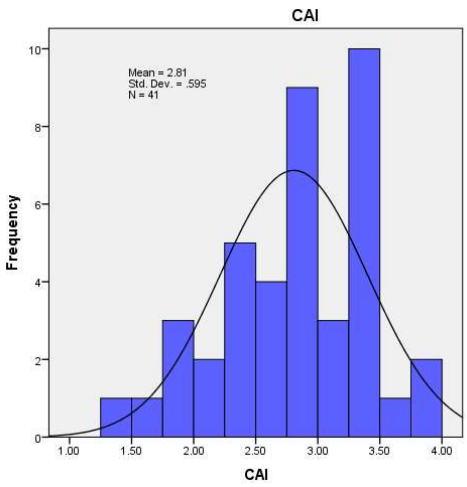
CAI
Mean = 2.81
Std. Dev. = .595
N = 41
Frequency
CAI

(l)

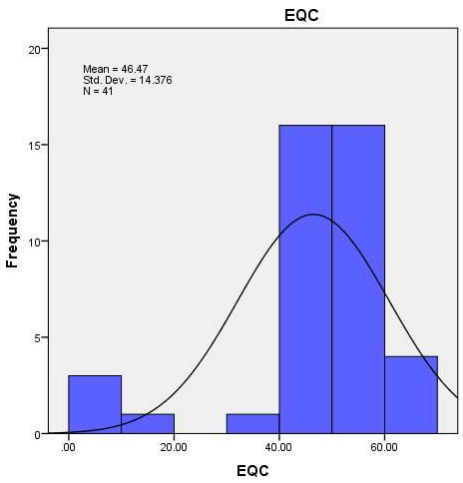
EQC
Mean = 46.47
Std. Dev. = 14.376
N = 41
Frequency
EQC

(m)

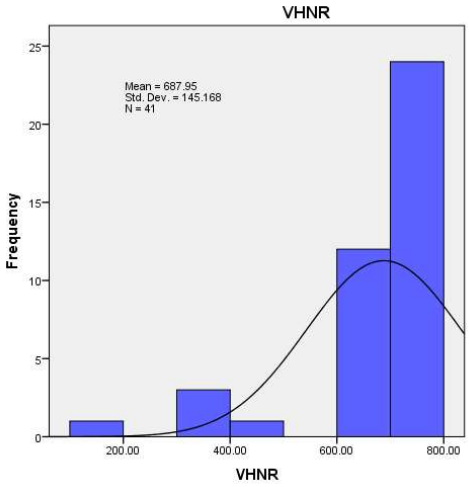
VHNR
Mean = 687.95
Std. Dev. = 145.168
N = 41
Frequency
VHNR

(n)

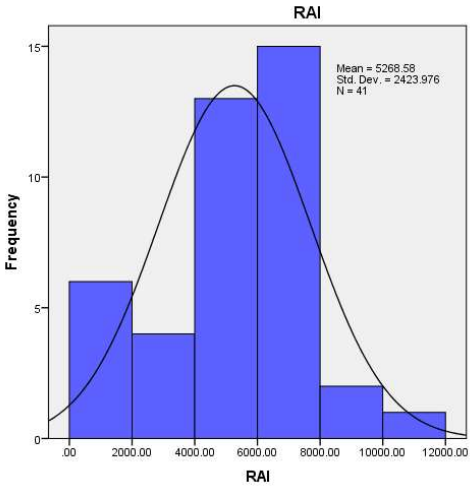
RAI
Mean = 5268.58
Std. Dev. = 2423.976
N = 41
Frequency
RAI

(o)

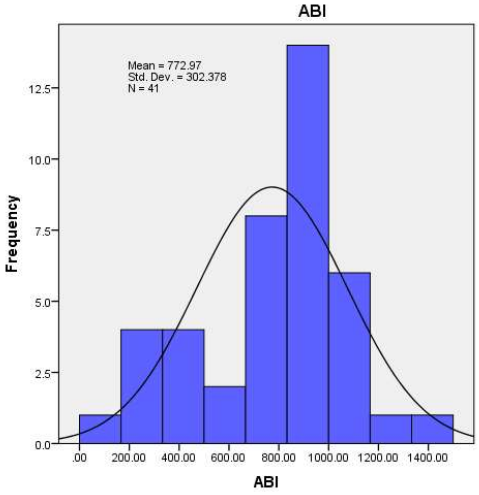
ABI
Mean = 772.97
Std. Dev. = 302.378
N = 41
Frequency
ABI

(p)

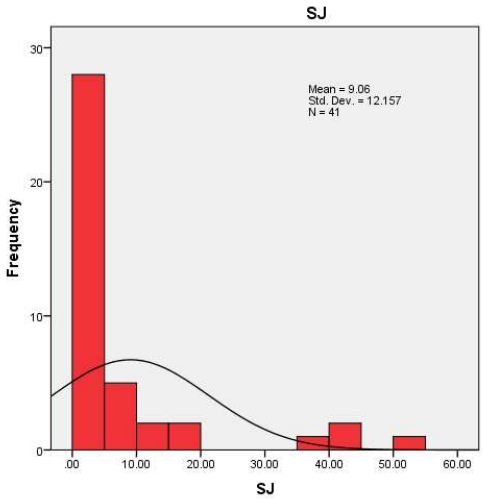
SJ
Mean = 9.06
Std. Dev. = 12.157
N = 41
Frequency
SJ

(q)

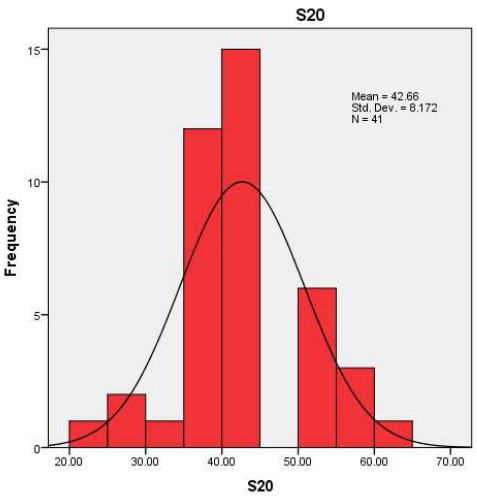
S20
Mean = 42.66
Std. Dev. = 8.172
N = 41
Frequency
S20

(w)

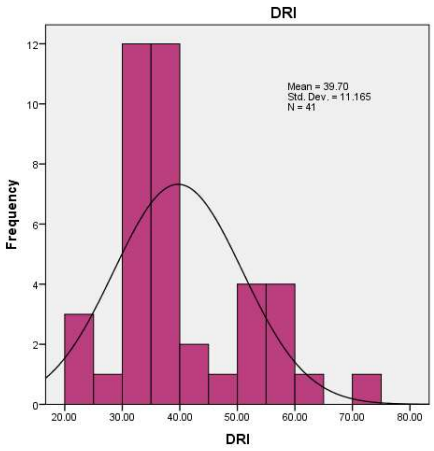

(z)

Figure 30. Frequency distribution of input variables used in predicting DRI

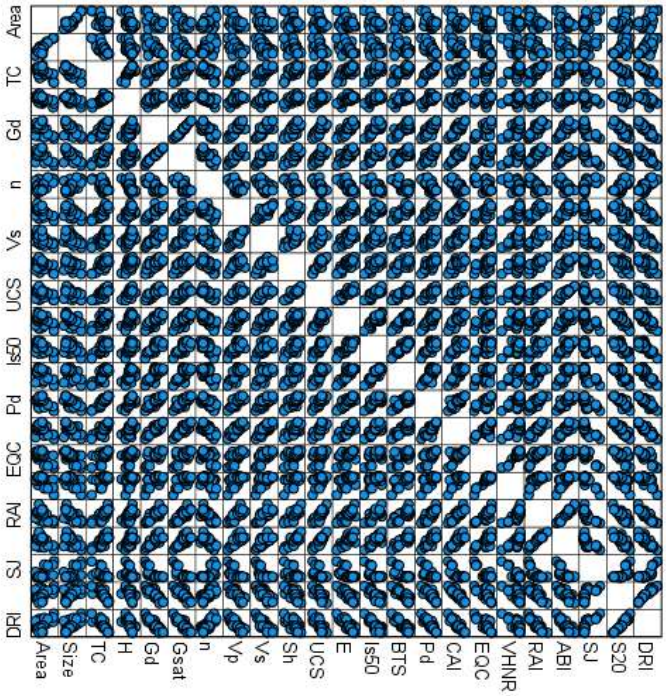

Figure 31. Scatter plot of total parameters

Statistical analyses and Machine learning Results

Statistical analysis

In this study, a comprehensive statistical analysis was conducted to examine the relationships between fabric features, physical and mechanical abrasivity properties, and drillability of the rock samples. Both linear and nonlinear regression techniques, along with bivariate correlation analysis, were employed to identify potential associations between petrographic characteristics, engineering properties, and the Drilling Rate Index (DRI). The statistical results were carefully evaluated to determine the strength and significance of these relationships and to identify the most suitable predictive models capable of representing the interactions between DRI,

mineralogical features, and mechanical behavior. This approach provided a thorough understanding of the factors controlling rock drillability and abrasiveness, offering valuable insights for geotechnical, mining, and construction applications where accurate prediction of rock performance is essential

Pearson's correlation coefficient

Pearson's correlation coefficient (R) was applied to study the efficiency and significant correlation between DRI with petrographical, textural, and engineering features.

The resulting statistical outcomes were thoroughly evaluated to select the most robust predictive models. The strength of associations among these variables was assessed using Pearson's correlation coefficient (R), as defined in Equation 13.

$$Rxy = \frac{COVxy}{SxSy} \tag{13}$$

The mean absolute error (MAE) and root mean square error (RMSE) were also implemented for evaluating each model; these metrics are calculated according to Equations 14 and 15, respectively.

$$MAE = \frac{\sum_{i=1}^{n}|Y_i - X_i|}{n} \tag{14}$$

$$RMSE = \sqrt{\frac{1}{n}\sum_{i=1}^{n}(Y_i - X_i)^2} \tag{15}$$

Let Yi be the measured value, Xi be the predicted value, and n be the number of observations. The optimal model fit is characterized by the following conditions: RMSE = 0, AME = 0, and $R^2 = 1$.

To evaluate correlations between variables, the covariance was normalized by dividing it by the product of the standard deviations of the respective variables in each regression model. Table 10 presents the Pearson's correlation coefficients (R) quantifying the relationships among DRI and various physical, mechanical, and abrasivity properties. The statistical significance of each correlation coefficient was assessed using hypothesis testing based on P-values, following the approach recommended by Johnson (1998). A P-value less than 0.05 was considered indicative of statistical significance at a 95% confidence level.

There is a significant correlation between DRI and engineering properties, as indicated by P values of physical, mechanical, Abrasivity, and drillability properties which are less than 0.05 (Table 10).

The Fabric feature, physical, mechanical, abrasivity property, and drillability parameters analysis results showed a good correlation with Drilling Rate Index (DRI) in igneous rocks. As is observed in Table 10, a positive correlation exists between area, size, porosity, S_J, and S_{20} in igneous rocks and a negative correlation exists between dry and saturated density, UCS, E, Is_{50}, BTS, V_P, V_S, P_d, EQC, RAI, ABI, and CAI with Drilling Rate Index (DRI) generally. This trend was also observed by Yarali and Soyer (2013), Yenice et al. (2018), and Karrari et. al. (2022).

As shown in Table 10, strong negative correlations ($|R| > 0.80$) were observed between the Drilling Rate Index (DRI) and several physical, mechanical, and abrasivity-related parameters, including thermal conductivity (TC), dry density (ρ_d), saturated density (ρ_{sat}), P-wave velocity (Vp), uniaxial compressive strength (UCS), elastic modulus (E), point load strength index (Is_{50}), Brazilian tensile strength (BTS), punch strength index (P_d), Rock Abrasivity Index (RAI), Cerchar Abrasivity Index (CAI), Abrasivity Index (ABI), Sievers' J-value (S_J), and brittleness index (S_{20}). These negative correlations indicate an inverse relationship, whereby increasing rock strength, stiffness, density, and abrasivity generally result in lower drillability in igneous rocks. Similar trends have been reported by Hosseini et al. (2015), Yenice et al. (2018), Yenice (2019), and Karrari et al. (2022).

Table 10. Pearson correlation coefficient between DRI and petrographical features and Geotechnical properties of the studied rocks

		Physical characteristics					Mechanical characteristics					
		ρ_d (gr/cm^3)	ρ_{sat} (gr/cm^3)	n (%)	Vp (m/s	Vs (m/s)	Schmitt Hammer	UCS (MPa)	E (GPa)	Is_{50} (MPa)	BTS (MPa)	P_d (MPa)
DRI	Pearson Correlation	-0.89**	-0.87**	0.76**	-0.86**	-0.79**	-0.69**	-0.81**	-0.83**	-0.85**	-0.87**	-0.89**
	Sig. (2-tailed)	0.00	0.00	0.00	0.00	0.00	0.00	0.00	0.00	0.00	0.00	0.00
	N	41	41	41	41	41	41	41	41	41	41	41
		Fabric features					Abrasivity indices					Drillability peoperties
		Area (mm^2)	size (mm)	TC	H	CAI	EQC (%)	VHNR	RAI	ABI	S_J	S_{20}	DRI
DRI	Pearson Correlation	0.54**	0.60**	-0.84**	-0.66**	-0.90**	-0.73**	-0.71**	-0.90**	-0.88**	0.81**	0.96**	1
	Sig. (2-tailed)	0.00	0.00	0.00	0.00	0.00	0.00	0.00	0.00	0.00	0.00	0.00	
	N	41	41	41	41	41	41	41	41	41	41	41	41

The strongest correlations ($|R| \geq 0.90$) were identified between DRI and CAI ($R \approx -0.90$) as well as between DRI and RAI ($R \approx -0.90$), highlighting the dominant influence of rock abrasivity and surface hardness on drillability. These results confirm that rock strength and abrasivity are key controlling factors for drilling performance in hard igneous formations.

Consistent with Yenice et al. (2018), uniaxial compressive strength (UCS) shows a significant influence on DRI, as rock strength is a fundamental parameter governing drilling resistance. Furthermore, elastic modulus exhibited a stronger correlation with the Sievers' J-value (S_J) than with the brittleness index (S_{20}). This behavior can be explained by the fact that the S_J test mechanism more closely simulates the action of rotary drilling, making its relationship with elastic stiffness conceptually meaningful. Similar observations were previously reported by Kahraman et al. (2003).

In addition, the Cerchar Abrasivity Index (CAI) demonstrated a higher correlation with SJ than with S_{20}, which is expected since both CAI and S_J are strongly related to rock hardness and surface resistance. Comparable findings were also reported by Karrari et al. (2022), who showed that density, UCS, Is_{50}, and abrasivity indices significantly affect DRI in hard rock formations.

The weakest correlations in this study were observed between fabric-related parameters (such as mineral grain size and area proportions) and DRI. This may be attributed to the indirect influence of fabric features, which are primarily reflected through mineralogical composition rather than directly controlling drilling performance.

Subsequently, regression analyses were conducted to quantify the relationships between DRI and selected rock engineering properties. Since the relationships between the dependent variable (DRI) and independent variables are not necessarily linear, curve estimation techniques were applied to identify the most suitable nonlinear models, as recommended by Norusis (2002).

Simple regression analysis

In the following, the relationships between the Drilling Rate Index (DRI) and the engineering properties of the rocks were examined. Since the relationship between the dependent and independent variables is not necessarily linear, nonlinear (curve) estimation methods were applied (Norusis, 2002). Six regression models were considered for both linear and nonlinear analyses, including in Table 11.

In these equations, X is the independent variable such as fabric features, physical and mechanical abrasivity properties, C is a constant, and a_1 and a_2 are regression coefficients. The efficiency of each statistical model was evaluated using standard techniques, including the coefficient of determination (R^2), adjusted R^2 (Adj R^2), analysis of variance (ANOVA), and standard error (Std. Er). The R^2 and Adj R^2 values were used to assess the validity of the regression models, where higher R^2values (with a maximum of 1) indicate stronger relationships in linear regression. However, while R^2 is a useful indicator, it alone is not sufficient for comparing the performance of different regression models (Omar, 2016). Therefore, two additional error metrics were employed: The Mean Absolute Error (MAE) and the Root Mean Square Error (RMSE), calculated using Equations 14 and 15, respectively. Simple regression analyses were performed to investigate the relationships between petrographic, physical, and mechanical characteristics and the Drilling Rate Index (DRI). Simple regression analyses were conducted to evaluate the relationships between the DRI and various engineering properties of the granitic rocks. The performance of each regression equation was assessed using the coefficient of determination (R^2), adjusted R^2, ANOVA significance, and error indices including RMSE, MAE, and MSE (Table 12).

Among all examined models, Equation 34 represents the best regression relationship between DRI and the corresponding engineering parameter. This model exhibits an exceptionally high correlation coefficient (R = 0.98), with R^2 and adjusted R^2 values of 0.95, indicating that approximately 95% of the variation in DRI is explained by the independent variable. In addition, this equation has the lowest RMSE (2.94) and lowest MSE (8.63) among all models, confirming its superior predictive accuracy. The very high F-value (724.14) and statistically significant p-value (<0.001) further demonstrate the robustness and reliability of this regression.

Other strong-performing models include Equations 31, 28 (second), 27, 33, and 20, which show R^2 values ranging from 0.79 to 0.82 and relatively low RMSE values (approximately 4.8–5.2). These equations can be classified as very good predictive models, indicating strong nonlinear relationships between DRI and the examined engineering features.

Equations such as 17, 20, 22, 25, 26, 27, and 32 fall into a moderate to good performance category, with R^2 values between 0.66 and 0.77. While these models demonstrate statistically significant relationships ($p < 0.001$), their higher RMSE and MAE values indicate increased prediction uncertainty compared to the best-performing equations. These models may still be useful for preliminary estimations or comparative analyses but are less accurate for precise prediction of DRI.

The lowest regression performance is observed in Equations 16 and 17, which display R^2 values of 0.29 and 0.36, respectively, along with the highest RMSE and MSE values. These low coefficients of determination indicate weak explanatory power, suggesting that the corresponding engineering parameters have limited influence on DRI or that the relationship cannot be adequately captured using these simple regression forms. As a result, these equations are not recommended for predictive purposes.

Table 11. The regression models were considered for both linear and nonlinear analyses

No	regression models	Equation
1	Linear	$DRI = a_1.X + C$
2	Inverse	$DRI = \frac{a_1}{X} + C$
3	Logarithmic	$DRI = a_1.Ln(X) + C$
4	Quadratic	$DRI = a_1.X + a_2.X^2 + C$
5	Exponential	$DRI = \mathrm{Exp}(a_1.X).C$
6	Power	$DRI = X^{a_1} + C$

Table 12. Summary of the best-performing simple regression models relating DRI to engineering properties of granitic rocks

Equation Number	Equation	Model Summary				ANOVA		RMSE	MAE	MSE
		R	R^2	Adjusted R^2	Std. Error of the Estimate	F	Sig.			
16	$DRI = 54.47 \times Area + 30.6$	0.54	0.29	0.27	9.51	16.17	0.00	9.23	-1.1	85.10
17	$DRI = 45.65 \times Size + 26.12$	0.60	0.36	0.34	9.05	21.86	0.00	8.81	-0.93	77.52
17	$DRI = -35.81 \times TC + 102.01$	0.84	0.70	0.69	6.21	90.34	0.00	6.06	0.00	36.67
18	$DRI = -27.42 \times H + 88.91$	0.66	0.43	0.42	8.52	29.73	0.00	8.31	0.00	69.01
19	$DRI = -15.09 \times \rho_d + 448.12$	0.89	0.80	0.79	5.05	156.36	0.00	4.93	0.00	24.28
20	$DRI = -15.82 \times \rho_{Sat} + 470.25$	0.87	0.75	0.74	5.66	116.81	0.00	5.52	-0.01	30.44
21	$DRI = 33.59 \times n + 10.00$	0.76	0.58	0.57	7.30	54.61	0.00	7.12	0.00	50.67
22	$DRI = -0.03 \times Vp + 227.61$	0.86	0.73	0.73	5.85	106.94	0.00	6.07	-2.07	36.82
23	$DRI = -0.06 \times Vs + 216.66$	0.79	0.62	0.61	6.98	63.33	0.00	6.85	0.76	46.93
24	$DRI = -34.08 \times Ln(SH) + 172.98$	0.70	0.48	0.47	8.13	36.41	0.00	7.93	0.00	62.90
25	$DRI = -0.28 \times UCS + 69.79$	0.81	0.66	0.65	6.64	74.13	<0.001	6.47	0.00	41.93
26	$DRI = -26.00 \times Ln(E) + 133.18$	0.83	0.69	0.68	6.32	85.76	<0.001	6.17	0.02	38.02
27	$DRI = -31.23 \times Ln(IS50) + 97.81$	0.87	0.75	0.75	5.61	119.55	<0.001	14.07	4.46	197.91
26	$DRI = -30.60 \times Ln(BTS) + 120.53$	0.87	0.75	0.75	5.63	118.11	<0.001	13.11	4.46	171.71
27	$DRI = -2.09 \times Pd + 81.92$	0.89	0.79	0.79	5.13	150.51	<0.001	5.00	0.00	25.03
28	$DRI = -16.91 \times CAI + 87.16$	0.90	0.81	0.81	4.89	169.47	<0.001	4.77	0.00	22.75
29	$DRI = -0.57 \times EQC + 66.24$	0.74	0.54	0.53	7.66	45.93	<0.001	7.47	0.01	55.85
30	$DRI = -0.06 \times VHNR + 77.49$	0.71	0.51	0.50	7.91	40.62	<0.001	7.72	-0.04	59.58
31	$DRI = -0.004 \times RAI + 61.65$	0.91	0.82	0.81	4.82	175.19	<0.001	4.80	0.87	23.07
32	$DRI = -0.032 \times ABI + 64.76$	0.88	0.77	0.77	5.41	131.23	<0.001	5.29	0.32	27.98
33	$DRI = 11.59 \times Ln(SJ) + 19.76$	0.89	0.79	0.78	5.20	145.29	<0.001	5.07	0.00	25.74
34	$DRI = 0.23 \times S20\text{^}1.368$	0.98	0.95	0.95	0.06	724.14	<0.001	2.94	-0.13	8.63

The variation in model performance reflects the complex and nonlinear nature of rock drillability. High-performing equations typically involve parameters that directly control drilling resistance, such as brittleness, abrasivity, and strength-related indices, which have been shown to strongly influence DRI. Poorer models are likely associated with parameters that have indirect or secondary effects on drilling performance or are influenced by multiple interacting factors not fully represented in a single-variable regression.

The strong regression relationships obtained in this study are consistent with findings reported worldwide. Previous studies have shown that regression models predicting DRI or drilling performance commonly yield R^2 values between 0.70 and 0.90 for well-selected mechanical and abrasivity parameters (Bruland, 1998; Kahraman, 2002; Rostami et al., 2014). The exceptionally high R^2 value achieved by Equation 34 (0.95) exceeds many values reported in the literature, indicating that the selected parameter provides an excellent representation of drillability for the studied granitic rocks. Similar nonlinear regression approaches have been successfully applied in tunneling and mining projects worldwide, confirming the validity of the methodology used in this research.

Random Forest (RF) algorithm

The Random Forest (RF) algorithm is a widely used machine learning method employed across various engineering disciplines, including sea surface salinity assessment (Liu, at.al. 2015), groundwater pollution analysis (El Bilali, at al. 2021), and nanofluid research (Gholizadeh et

al. 2020, Jamei et al. 2021). This approach leverages an ensemble of Classification and Regression Trees (CART) and combines them through bagging to uncover complex, non-linear relationships between input and output variables.

While a single CART model can be susceptible to overfitting and instability, the Random Forest algorithm mitigates these weaknesses by constructing a multitude of independent decision trees and aggregating their results, thereby reducing error by averaging out the variances of individual weak classifiers. The independence of these trees is ensured through two key randomization techniques (Breiman, 2001).

The first technique involves training each tree on a randomly selected subset of the original training data, a process known as bootstrapping. If we denote a single decision tree as T, the training data as x, and a specific random subset as θ, the prediction of a single tree is T(x,θ). The final RF prediction is then computed as a simple average of the predictions from all n individual trees:

$$RF(x) = (1/n) * \Sigma\ Ti(x, \theta i)$$

The second technique (Breiman, 2001) introduces further randomness by restricting the split at each node within a tree to a random subset of the input features. Each tree identifies the most relevant variables from its available subset (Si) associated with the training data. The overall estimation of the Random Forest model for a given input is formally represented by the equation above, where the output for the training data is denoted by Ox.

To build each tree, the bootstrap method is used to create a training subset, and the CART method is applied, with the split at each node chosen from the randomly selected variable subset. In this study, the Random Forest model was applied to predict rip current event susceptibility. The model's key hyperparameters were set as follows: the number of trees (n_estimators) was 400, the maximum depth of individual trees (max_depth) was 5, and the maximum number of split subsets (max_leaf_nodes) was 5. The results of the quantitative evaluation of training phase are shown in Table 13.

As summarized in Table 4, the dataset comprises 41 igneous rock samples, including 26 monzogranite, 8 syenogranite, 5 quartz syenite, 1 granodiorite, and 1 quartz monzonite. In the Random Forest (RF) modeling, the dataset was divided into training and testing subsets following the workflow illustrated in Figure 6. A random data-splitting strategy was applied, whereby approximately 70% of the samples were used for model training and the remaining 30% were reserved for independent testing. The random allocation was performed to ensure that the different rock groups were reasonably represented in both subsets. This procedure enabled effective model training while allowing an unbiased evaluation of the predictive performance of the RF model.

Figure 32a illustrates the qualitative performance of RF models in the training phase, and Figure 33b illustrates the qualitative performance of RF models in the testing phase.

According to Figure 32a, all the predicted values of DRI in the training phase were almost in the ±25% error line. As seen in Figure 32a, RF had no required capability of predictions DRI =2.5–5 in comparison with other soft computing models. The RF model demonstrated exceptional performance (R = 0.996, R^2=0.99, RMSE = 1.10), significantly outperforming traditional empirical correlations. The proposed RF model in this research (R^2 = 0.99) significantly outperforms the best previously published empirical model by Yarali and Soyer (2013) (R^2 = 0.78).

Table 13. Performance of various ML models for prediction of DRI.

Model	Training					Testing				
	Number of Samples for training	R	R^2	RMSE	MAPE	Number of Samples for testing	R	R^2	RMSE	MAPE
RF	28	0.9928	0.98	1.4694	2.03	13	0.9958	0.99	1.10	3.01

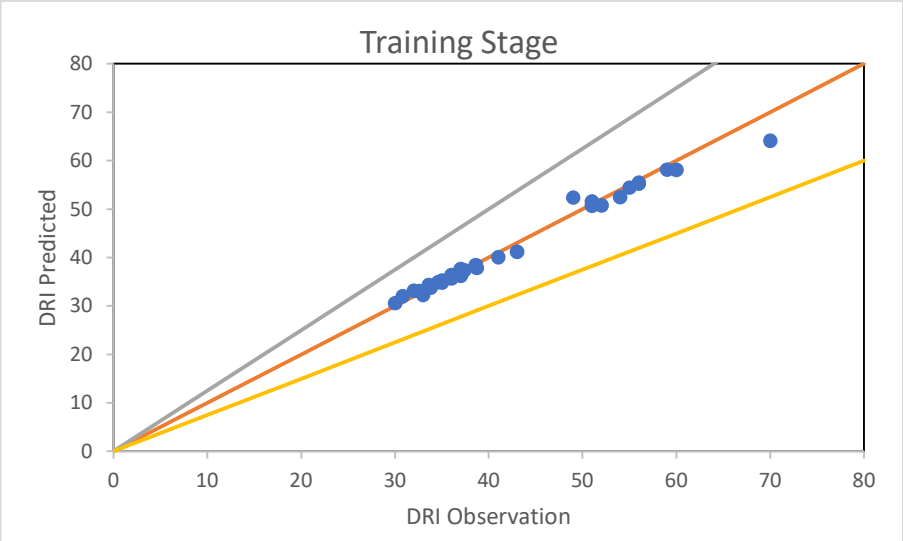

Figure 32 a. The Performance of RF model in the prediction of DRI for training phase

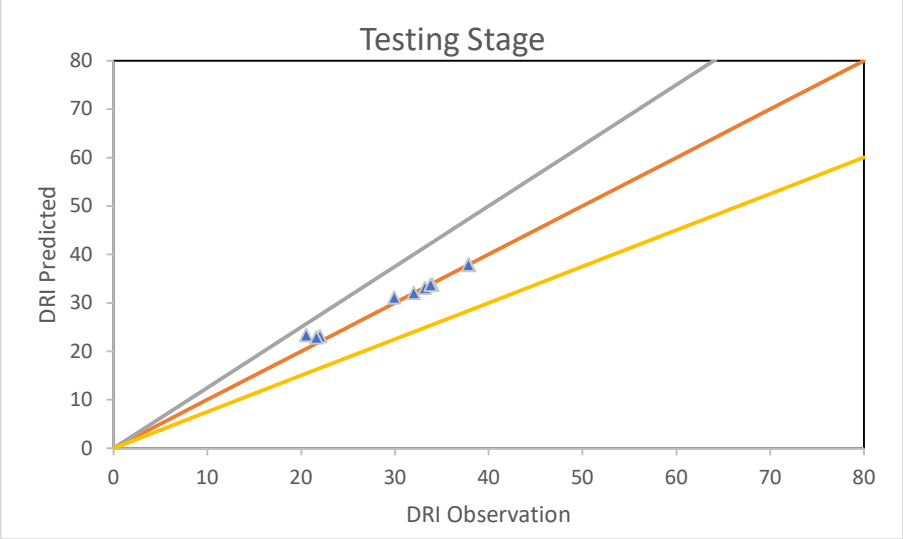

Figure 32 b. The Performance of RF model in the prediction of DRI for testing phases

Artificial Neural Network (ANN)

The design of an Artificial Neural Network (ANN) architecture involves determining the optimal number of hidden layers and the number of processing elements (neurons) within them. This is typically an iterative process where various configurations are tested to identify the structure that yields the best predictive performance.

The number of neurons in the input layer is dictated by the number of features in the input vector, while the number of neurons in the output layer corresponds to the number of target variables to be predicted. In a standard feedforward network, each neuron is connected to every neuron in the subsequent layer, but no connections exist between neurons within the same layer.

Determining the precise number of neurons in the hidden layer is a complex task without a definitive analytical solution. A common rule of thumb suggests this number is a function of both the dimensionality of the input data and the complexity of the patterns to be learned, often related to the concept of linear separability. Consequently, identifying the optimal architecture remains an empirical process.

The ANN architecture was developed using a feedforward backpropagation algorithm. The optimal network structure was identified through a trial-and-error process conducted in the MATLAB environment. The final architecture consisted of 22 neurons in the input layer, corresponding to the selected geotechnical and mineralogical parameters, a single hidden layer with 10 neurons, and one output neuron representing the predicted DRI value (Figures 33, and 6).

To ensure stable and efficient training by preventing extreme values from disproportionately influencing the network's weights, all input and output data were normalized to a range between 0 and 1 using a min-max scaling approach, as defined by Relationship 34.

$$X_i = 2\left(\frac{X - X_{\min}}{X_{\max} - X_{\min}}\right) - 1 \quad (34)$$

The developed model is evaluated based on the highest correlation coefficient and the least RMSE value. The values of MSE, R, R^2 are also presented in Table 14.

Considering Figure 34 (neural network results), the Determination coefficient of DRI with physical, mechanical, and mineralogical parameters, abrasivity, and drillability indices is reported as 0.98.

The results of RF models showed that the Determination coefficient of DRI with those parameters is 0.99. Thus, RF have high precision in the estimation of the static properties. Similar results (high efficiency of this method in the prediction of static parameters) have also been reported by other researchers as (Singh et al., 2004, Madhubabu et al., 2016, , and Kahraman et al., 2010).

In order to have a better investigation on the actual and predicted values for DRI, the corresponding graphs were prepared which has been shown in Figure 34.

Discussion

This study successfully developed and validated a robust Random Forest (RF) model for predicting the Drilling Rate Index (DRI) of igneous rocks, demonstrating the significant potential of ensemble machine learning in geotechnical engineering. The proposed model achieved exceptional predictive accuracy, with a Determination coefficient (R^2) of 0.99 and a root mean square error (RMSE) of 1.10 on the testing set. This performance underscores the model's reliability and its practical utility for drillability assessment in hard rock formations.

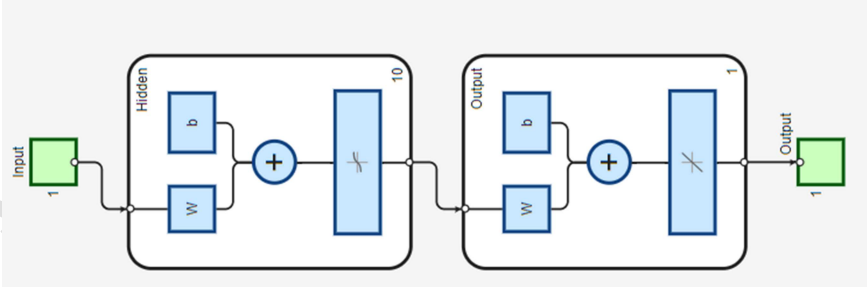

Figure 33. The architecture of the used network in ANN

Table 14 Performance of various ANN models for prediction of DRI

Model	Observation (Number of Samples)	MSE	R	R^2
Training	25	0.0002	1.00	1.00
Validation	8	6.92	0.9798	0.96
Test	8	4.00	0.9881	0.97

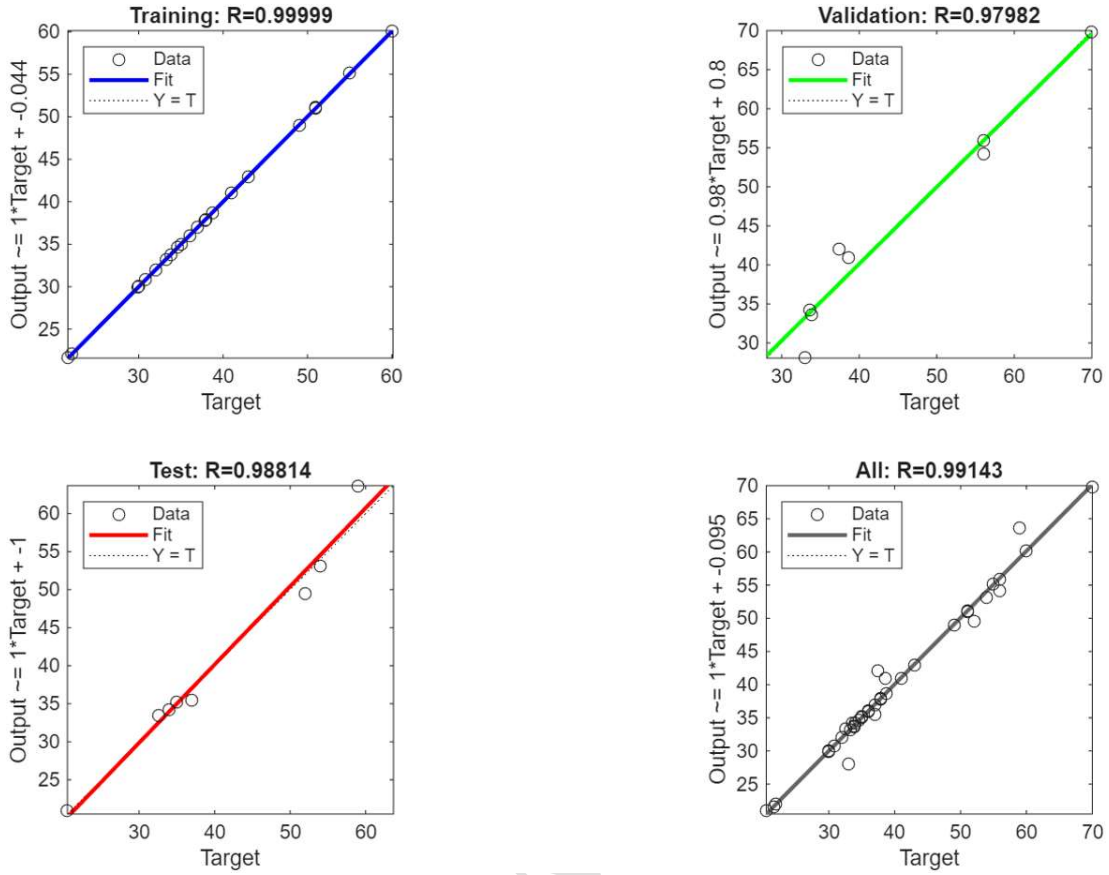

Figure 34. DRI prediction process in neural network in this study a) Training results b) validation results c) test results, d) all results

Model Performance and Validation

The regression analyses revealed that DRI exhibits strong nonlinear relationships with several engineering properties, particularly brittleness indices, abrasivity indicators, and hardness-related parameters. Among the regression models evaluated, nonlinear models generally outperformed linear models, confirming the complex interactions among rock properties influencing drillability. The best regression models achieved R^2 values in the range of 0.79–0.95, which is consistent with values reported in previous studies on granitic rocks, where R^2 typically ranges between 0.70 and 0.90 for well-selected predictors (Bruland, 1998; Kahraman, 2002; Rostami et al., 2014).

The machine learning models demonstrated superior predictive performance compared to regression models. The Random Forest (RF) model, in particular, achieved the highest R^2 (>0.99) with the lowest RMSE and MAE values, indicating excellent agreement between predicted and measured DRI. These results validate the ability of RF to capture complex, nonlinear interactions among multiple engineering and petrographic variables, consistent with recent studies highlighting the robustness of ensemble learning in rock mechanics applications (Zhang et al., 2020; Li et al., 2020). ANN models also performed well, providing reliable predictions with slightly higher error indices, reflecting the sensitivity of neural networks to dataset size and network architecture. Overall, the comparison with previous literature confirms that machine learning techniques, especially RF, offer significant advantages in predicting rock drillability over conventional regression approaches.

The RF model developed in this study represents a substantial improvement over traditional

empirical and regression-based approaches (Table 15). To contextualize this advancement, a comparative analysis with previously published models is presented in Table 16. Unlike conventional models that rely on limited parameters–primarily uniaxial compressive strength (UCS) and Brazilian tensile strength (BTS)–our model integrates a comprehensive suite of 22 inputs, including critical mineralogical (EQC, VHNR) and abrasivity (CAI, RAI, ABI) indices. This holistic approach allows the RF algorithm to capture complex, non-linear interactions that simpler linear or power-law regressions cannot.

Table 15 summarize the predictive performance of the RF and ANN models on the testing and training datasets, respectively. As expected, both models show higher R^2 and lower RMSE values for the training dataset compared to the testing dataset, indicating good learning capability without severe overfitting. The RF model outperformed the ANN model in both training and testing phases, demonstrating higher predictive accuracy and better generalization for DRI estimation.

The superior performance of the RF model ($R^2 = 0.99$) compared to the best previous model ($R^2 = 0.83$ by *Karrari et al., 2022*) highlights the advantage of using an ensemble machine learning algorithm capable of modeling complex, high-dimensional relationships. Furthermore, the model's high accuracy on the independent testing set confirms its robustness and generalizability within the domain of igneous rocks.

Dominant Controlling Factors and Novelty

Correlation analysis revealed that abrasivity indices–specifically the Cerchar Abrasivity Index (CAI) and Rock Abrasivity Index (RAI)–exhibited the strongest inverse relationships with DRI ($R > |0.90|$). This finding underscores that rock hardness and mineralogical resistance to wear are the dominant factors controlling drillability in hard, abrasive granitic formations, surpassing the influence of standalone strength measures like UCS.

Table 15. Comparative performance of DRI prediction models in this study

Model	Performance Metric	Value	Number of Samples Used for Training / Testing
RF	R^2	0.99	28 / 13
	RMSE	1.01	28 / 13
ANN	R^2	0.98	25 / 8
	RMSE	2.01	25 / 8

Table 16. Comparative performance of DRI prediction models

Study	Model Type	Key Input Parameters	R^2	RMSE	Rock Types Covered
Yarali & Soyer (2013)	Linear Regression	UCS, BTS, SRH, SSH	0.78	-	Sedimentary, Metamorphic, Igneous
Yenice et al. (2018)	Multivariate Regression	UCS, BTS, P-wave velocity	0.74	-	Granite, Basalt
Karrari et al. (2022)	Regression	Density, UCS, IS_{50}, ABI	0.83	-	Granite
This Study	**Random Forest (RF)**	**UCS, EQC, VHNR, CAI, RAI, ABI, TC, V_P, V_S, etc. (22 parameters)**	**0.99**	**1.10**	**Igneous (Granitic ROCK)**

The principal novelty of this research lies in the successful integration of quantitative mineralogical and petrographic data into a predictive machine learning framework. While traditional models have historically relied on a narrow set of physical and mechanical properties, this study demonstrates that fabric features (Texture Coefficient - TC), equivalent quartz content (EQC), and composite hardness (VHNR) are paramount for accurate DRI estimation. This paradigm shifts from empirical regression to a data-driven, multi-parameter ML model addresses a significant gap in the existing body of knowledge.

Empirical and predictive models are considered practically useful when they contribute to reducing time, cost, and operational uncertainty in engineering applications. While it is well recognized that incorporating a larger number of influential parameters may naturally increase correlation coefficients, the objective of this study is not merely to maximize statistical correlation, but to evaluate the reliability and applicability of different modeling approaches for DRI estimation. The proposed models aim to integrate laboratory-measured parameters into a unified predictive framework, thereby reducing the need for repeated and time-consuming drillability tests during project planning and preliminary design stages.

In contrast to conventional regression analysis, machine learning models such as Artificial Neural Networks (ANN) and Random Forest (RF) are capable of capturing complex nonlinear interactions among multiple variables without requiring strict assumptions regarding functional form. This advantage is particularly important for DRI estimation, where rock drillability is governed by the combined effects of physical, mechanical, mineralogical, and abrasivity properties. Accordingly, machine learning approaches were employed to complement regression analysis and to provide more robust predictive performance, especially in cases where regression models failed to satisfy statistical significance criteria.

Influence of Rock Type and Model Limitations

The dataset comprised 41 samples classified into six igneous rock groups: Monzogranite, Quartz Syenite, Syenogranite, Quartz Monzonite, Granodiorite, and others. An analysis of model performance across these groups indicates consistent predictive accuracy, suggesting that the selected parameters effectively capture the drillability determinants common to felsic igneous rocks. However, the model's performance was marginally better for the more abundantly sampled Monzogranite and Syenogranite. This highlights that while the model is robust within the studied spectrum, its precision is inherently tied to the representativeness of the training data for each subtype.

Rock-Type Specificity: The model is explicitly developed and validated for igneous rocks, particularly granitic types. Its direct application to sedimentary or metamorphic rocks is not recommended without further validation and potential retraining with appropriate data, as the controlling parameters and their relationships may differ fundamentally.

Dataset Size and Diversity: While sufficient for robust model development, the dataset of 41 samples, though comprehensive in parameters, is moderate in size. Performance is optimal for rock types well-represented in the training set (e.g., Monzogranite). Expanding the database to include a wider variety of igneous subtypes (e.g., gabbro, basalt) and a greater number of samples would enhance the model's generality and reliability.

Inherent ML Constraints: The RF model, while highly accurate, operates as a "black box." The complex interplay of variables makes it difficult to extract simple, universal physical laws from the model structure, unlike transparent regression equations.

Laboratory to Field Translation: The model predicts laboratory-scale DRI. While this is a

crucial indicator, field drilling rates are also influenced by in-situ conditions (rock mass fracturing, groundwater, stress state) and machine parameters, which are not accounted for in the current model.

Practical Implications and Future Work

The developed RF model provides a practical, data-driven tool for geologists and engineers to reliably forecast drilling performance during the preliminary planning of tunneling and mining projects in granitic terrains. This can lead to optimized cutterhead design, improved tool life predictions, better cost estimation, and more efficient project scheduling.
To build upon this work, future research should focus on:

Expanding the database to include a broader range of igneous, metamorphic, and sedimentary rocks to develop more universal or rock-class-specific models.

Incorporating in-situ rock mass parameters (e.g., fracture frequency, rock quality designation) to bridge the gap between laboratory indices and field-scale tunneling performance.

Applying explainable AI (XAI) techniques such as SHAP (SHapley Additive exPlanations) analysis to quantify the contribution of each input variable, enhancing the interpretability of the model and providing deeper insights into the physics of rock drillability.

Exploring real-time adaptation by integrating the model with data from monitoring-while-drilling (MWD) systems to enable dynamic prediction and adjustment during excavation.

Conclusion

This study successfully investigated the drillability of hard granitic rocks by establishing a robust, data-driven framework that integrates extensive experimental characterization with advanced predictive modeling. A comprehensive suite of petrographic, physical, mechanical, and abrasivity parameters was measured for 41 igneous rock samples. These data were used to develop and compare conventional nonlinear regression models and modern machine learning algorithms-Artificial Neural Networks (ANN) and Random Forest (RF).

The analysis confirms that rock drillability is governed by complex, nonlinear interactions among a multitude of factors, including brittleness, hardness, abrasivity, and mineralogical composition. While nonlinear regression models effectively captured these relationships, achieving R^2 values up to 0.95-consistent with established studies (Bruland, 1998; Kahraman, 2002; Rostami et al., 2014), the ensemble Random Forest (RF) algorithm demonstrated superior predictive capability. The RF model achieved exceptional performance, with the coefficient of determination (R^2) of $R^2 > 0.99$ and significantly lower error indices (RMSE = 1.1) on the testing set, validating its effectiveness in modeling the intricate, high-dimensional relationships within the data.

A key finding, supported by correlation analysis, is the dominance of abrasivity indices—specifically the Cerchar Abrasivity Index (CAI) and Rock Abrasivity Index (RAI)—which exhibited the strongest inverse correlations ($R > |0.90|$) with the Drilling Rate Index (DRI). This underscores that rock hardness and mineralogical wear resistance are paramount in controlling drillability, surpassing the predictive power of standalone strength measures. The study further highlights the influence of rock type, as variations in quartz content, grain size, and texture among the six granitic groups impacted model accuracy. This suggests that incorporating lithology as a feature or developing group-specific models could further refine predictions.

The principal novelty and contribution of this work lie in its paradigm-shifting methodology. It moves beyond traditional strength-based empirical models by successfully integrating quantitative mineralogical and petrographic data into a powerful machine learning framework.

This approach addresses a significant gap in the literature and provides a substantially more accurate tool for DRI prediction in igneous rocks.

The study acknowledges certain limitations. The model is developed on a laboratory-scale dataset from a specific geological context, which may affect direct applicability to other regions or in-situ field conditions where rock mass properties play a crucial role. Furthermore, data-driven models like RF, while highly accurate, offer limited explicit insight into causal physical relationships. Future research should focus on: (1) expanding the database to include a wider variety of igneous, metamorphic, and sedimentary rocks to improve generality; (2) incorporating in-situ rock mass parameters to bridge the lab-field gap; (3) employing explainable AI (XAI) techniques to enhance model interpretability; and (4) exploring rock group–specific modeling strategies.

In summary, this research demonstrates that integrating comprehensive experimental testing with ensemble machine learning provides a robust and superior framework for predicting rock drillability. The developed RF model offers significant practical benefits for the planning stages of tunneling, mining, and construction projects in hard rock environments, enabling more reliable forecasting of drilling performance, optimization of equipment selection, and improvement of overall excavation efficiency and cost-effectiveness.

Acknowledgments

The technical and logistical support provided by the Department of Geology at Ferdowsi University of Mashhad, as well as the management of the KSWCT project in facilitating the sample collection, are greatly appreciated.

Funding: This research received no external funding.
Institutional Review Board Statement: Not applicable.
Informed Consent Statement: Not applicable.

Data Availability Statement

Data that support the findings of this study are available from the corresponding author upon reasonable request

Conflicts of Interest
The authors declare no conflicts of interest.

Ethical approval
All procedures performed in studies do not involve human/animal participants.

References

AFNOR. 2000. NF P 94-430 1. Détermination Du Povoir Abrasive D'une Roche- Partie 1: Essai DE Rayure Avec Une Pointe. Paris; 2000. (in French)

Ajalloeian, R., Kamani, M., 2019. An investigation of the relationship between Los Angeles abrasion loss and rock texture for carbonate aggregates. Bulletin of engineering geology and the environment, 78: 1555-1563.

Akcin, N.A., Muftuoglu, Y.V., Bas, N., 1994. Prediction of drilling performance for electro-hydraulic percussive drills. In: Proceedings of the Third International Symposium on Mine Planning and Equipment Selection, Balkema, Istanbul, Turkey, pp. 483-488

Åkesson, U., Stigh, J., Lindqvist, J. E., Göransson, M., 2003. The influence of foliation on the fragility of granitic rocks, image analysis and quantitative microscopy. Engineering Geology, 68: 275-288.

Akram, M. S., Farooq, S., Naeem, M., Ghazi, S., 2017. Prediction of mechanical behaviour from mineralogical composition of Sakesar limestone, Central Salt Range, Pakistan. Bulletin of Engineering Geology and the Environment, 76: 601-615.
Akün, M. E., Karpuz, C., 2005. Drillability studies of surface-set diamond drilling in Zonguldak region sandstones from Turkey. International journal of rock mechanics and mining sciences, 42: 473-479.
Alber, M., Kahraman, S., 2009. Predicting the uniaxial compressive strength and elastic modulus of a fault breccia from texture coefficient. Rock Mechanics and Rock Engineering, 42: 117.
Alber, M., 2008. Stress dependency of the Cerchar abrasivity index (CAI) and its effects on wear of selected rock cutting tools. Tunnelling and underground space technology, 23: 351-359.
Alber, M., Yaralı, O., Dahl, F., Bruland, A., Käsling, H., Michalakopoulos, T. N., Özarslan, A., 2014. ISRM suggested method for determining the abrasivity of rock by the CERCHAR abrasivity test. In The ISRM suggested methods for rock characterization, testing and monitoring, Cham: Springer International Publishing. 1:1-101
Aleman, V. P., 1981. A strata strength index for boom type roadheaders. Tunnels & Tunnelling International, 13: http://worldcat.org/issn/0041414X
Aligholi, S., Lashkaripour, G. R., Ghafoori, M., Azali, S. T., 2017. Evaluating the relationships between NTNU/SINTEF drillability indices with index properties and petrographic data of hard igneous rocks. Rock Mechanics and Rock Engineering, 50: 2929-2953.
Altindag, R., 2004. Evaluation of drill cuttings in prediction of penetration rate by using coarseness index and mean particle size in percussive drilling. Geotechnical & Geological Engineering, 22: 417-425.
Anon, Q., 1977. The description of rock masses for engineering purposes. Quarterly Journal of Engineering Geology, 10: 355-399.
Ataei, M., KaKaie, R., Ghavidel, M., Saeidi, O., 2015. Drilling rate prediction of an open pit mine using the rock mass drillability index. International Journal of Rock Mechanics and Mining Sciences, 73: 130-138.
Azzoni, A., Bailo, F., Rondena, E., Zaninetti, A., 1996. Assessment of texture coefficient for different rock types and correlation with uniaxial compressive strength and rock weathering. Rock Mechanics and Rock Engineering, 29: 39-46.
Bertini Junior, J. R., Lavi, B., 2025. Enhancing Rate of Penetration Prediction in Drilling Operations: A Data Stream Framework Approach. Available at SSRN 4790150.
Bieniawski, Z. T., 1975. The point-load test in geotechnical practice. Engineering geology, 9: 1-11.
Bilgin, N., Yazici, S., Eskikaya, S.,1996. A model to predict the performance of roadheaders and impact hammers in tunnel drivages. In ISRM EUROCK (pp. ISRM-EUROCK). ISRM.
Breiman, L., 2001. Random forests. Machine learning, 45: 5-32.
Bruland A., 2000. Hard rock tunnel boring. Drillability test methods Vol. 8, Ph.D. Thesis, Department of Civil and Transport Engineering, NTNU, Norwegian University of Science and Technology, Trondheim, Norway, p 250.
Bruland, A., 1998. Hard rock tunnel boring. Ph.D. Thesis, Norwegian University of Science and Technology, Trondheim.
Capik, M., Yilmaz, A. O., 2017. Correlation between Cerchar abrasivity index, rock properties, and drill bit lifetime. Arabian Journal of Geosciences, 10: 15-25.
Cerchar,1986. Centre d'Etudes et des Recherches des Charbonages de France, Verneuil (in French)
Comakli, R., Cayirli, S., 2019. A correlative study on textural properties and crushability of rocks. Bulletin of Engineering Geology and the Environment, 78: 3541-3557.
Dahl F., 2003. DRI, BWI, CLI and NTNU Standards. Angleggsdrift, Trondheim
Dahl, F. Bruland, A. Jakobsen, P.D. Nilsen, B., Grov, E., 2012. Classifications of properties influencing the drillability of rocks based on the NTNU/SINTEF test method. Tunnelling and Underground Space Technology, 28:150-158.
Dai, B., Gu, C., Zhao, E., Qin, X., 2018. Statistical model optimized random forest regression model for concrete dam deformation monitoring. Structural Control and Health Monitoring, 25:2160-2170.
Darbor, M., Faramarzi, L., Sharifzadeh, M., 2019. Performance assessment of rotary drilling using non-linear multiple regression analysis and multilayer perceptron neural network. Bulletin of Engineering Geology and the Environment, 78: 1501-1513.
Deere, D.U., Miller, R.P., 1966. Engineering classifications and index properties of intact rock. Technical Report AFWL-TR, 65-116. Air Force Weapons Laboratory, Kirtland Air Force Base,

Albuquerque, 300.
Duzgoren-Aydin, NS, Aydin A, Malpas J., 2002. Re-assessment of chemical weathering indices: Case study on pyroclastic rocks of Hong Kong. Engineering Geology 63: 99-119.
Ekincioglu G., Akbay D., 2021. Estimating the drilling rate index (DRI) values of rocks by indirect methods, 6nd International Conference on Material Science and Technology in Cappadocia (IMSTEC'21), Cappadocia/TURKEY.
Ekincioglu, G., Altindag, R., Sengun, N., Demirdag, S., Guney, A., 2013. The relationships between drilling rate index (DRI), physico-mechanical properties and specific cutting energy for some carbonate rocks. In ISRM EUROCK (pp. ISRM-EUROCK). ISRM. 12:10-25.
El Bilali, A., Taleb, A., Brouziyne, Y., 2021. Groundwater quality forecasting using machine learning algorithms for irrigation purposes. Agricultural Water Management, 245" 106625.
Ergen, F. and Katlav, M., 2024. Investigation of optimized machine learning models with PSO for forecasting the shear capacity of steel fiber-reinforced SCC beams with/out stirrups. Journal of Building Engineering, 83:108455.
Ersoy, A., Waller, M. D., 1995. Textural characterisation of rocks. Engineering geology, 39: 123-136.
Ezazi, M., Ghorbani, E., Shafiei, A., Sharifi Teshnizi, E., O'Kelly, B. C., 2024. Laboratory hydraulic tensile strength correlation with strength-based brittleness indices for carbonate reservoirs. Geosciences, 14: 52-65.
Farooq, F., Nasir Amin, M., Khan, K., Rehan Sadiq, M., Javed, M.F., Aslam, F. and Alyousef, R., 2020. A comparative study of random forest and genetic engineering programming for the prediction of compressive strength of high strength concrete (HSC). Applied Sciences, 10: p.7330.
Fattahi, H., Bazdar, H.,2017. Applying improved artificial neural network models to evaluate drilling rate index. Tunnelling and Underground Space Technology, 70: 114-124.
Fowell, R.J., McFeat-Smith, I., 1976. Factors influencing the cutting performance of a selective tunnelling machine. Tunnelling '76, Institution of Mining and Metallurgy, London, pp. 3-11.
Gholizadeh, M., Jamei, M., Ahmadianfar, I., Pourrajab, R., 2020. Prediction of nanofluids viscosity using random forest (RF) approach. Chemometrics and Intelligent Laboratory Systems, 201: 104010.
Hashemi, H., Yazdi, A., Teshnizi, E. S., 2025. Stability Analysis of the rock slope of Transfer and Kinematic analysis (The Case study of the Gabric Dam spillway trench head in south of Iran). Journal of Earth Statistic, 3:10-25.
Hassanpour, J., Rostami, J., Azali, S. T., Zhao, J., 2014. Introduction of an empirical TBM cutter wear prediction model for pyroclastic and mafic igneous rocks; a case history of Karaj water conveyance tunnel, Iran. Tunnelling and underground space technology, 43: 222-231.
Haykin, S., Lippmann, R., 1994. Neural networks, a comprehensive foundation. International Journal of Neural Systems, 5: 363-364.
Hemmati, A., Ghafoori, M., Moomivand, H., Lashkaripour, G. R., 2020. The effect of mineralogy and textural characteristics on the strength of crystalline igneous rocks using image-based textural quantification. Engineering Geology, 266: 105467.
Hoek, E., Brown, E.T., 1980. Underground Excavations in Rock. Institution of Mining and Metallurgy, London, 300.
Hosseini R., Lashkaripour G.R., Moghadas N.H., Ghafoori M., 2015. Estimation of S20-brittleness (an input parameter in drilling rate index, DRI) using other types of brittleness. 11th Iranian and 2nd Regional Tunnelling Conference Tunnels and the Future. 1-7
Howarth, D. F., Rowlands, J. C., 1987. Quantitative assessment of rock texture and correlation with drillability and strength properties. Rock mechanics and rock engineering, 20: 57-85.
Howarth, D. F., Adamson, W. R., Berndt, J. R., 1986. Correlation of model tunnel boring and drilling machine performances with rock properties. In International Journal of Rock Mechanics and Mining Sciences & Geomechanics Abstracts, 23: 171-175.
Huang, J., Duan, T., Zhang, Y., Liu, J., Zhang, J., Lei, Y., 2020. Predicting the permeability of pervious concrete based on the beetle antennae search algorithm and random forest model. Advances in Civil Engineering, 2020: p.8863181.
Huang, S. L., Wang, Z. W., 1997. The mechanics of diamond core drilling of rocks. International Journal of Rock Mechanics and Mining Sciences, 34: 134-146.
Hucka, V., Das, B., 1974. Brittleness determination of rocks by different methods. International Journal Rock Mechanics and Mining Sciences & Geomechanics Abstracts, 11: 389-392.

International Association of Engineering Geology (IAEG),1979. Classification of rocks and soils for engineering geological mapping: part I: rock and soil materials. Bulletin of the International Association of Engineering Geology, 19: 364-371.
Iqbal, M. M., Bakar, Z. A., 2016. Drillability Evaluation of Limestone Rock Quarries in Punjab and Khyber Pakhtunkhwa, Pakistan. Pakistan Journal of Engineering and Applied Sciences, 12:15-25.
ISRM, 2007. The complete ISRM suggested methods for rock characterization, testing and monitoring, 1974-2006, suggested methods prepared by the commission o testing methods, International Society for Rock Mechanics, R. Ulusay and J. A. Hudson (Eds.), Compilation Arranged by The ISRM Turkish National Group, Ankara, Turkey, 230.
ISRM, 1981. Rock characterization testing and monitoring ISRM suggested methods, suggested methods for determining hardness and abrasiveness of rocks. Part 3, 101-3.
Jamei, M., Karbasi, M., Olumegbon, I. A., Mosharaf-Dehkordi, M., Ahmadianfar, I., & Asadi, A. (2021). Specific heat capacity of molten salt-based nanofluids in solar thermal applications: A paradigm of two modern ensemble machine learning methods. Journal of Molecular Liquids, 335, 116434.
Jang, H., Topal, E., 2014. A review of soft computing technology applications in several mining problems. Applied Soft Computing, 22: 638-651.
Johnson, R., 1998. Elementary statistics. (5th Edition), PWS. KENT Publishing Company, Boston, USA, 350.
Kahraman, S., 1999. Rotary and percussive drilling prediction using regression analysis. International journal of rock mechanics and mining sciences, 36:981-989.
Kahraman, S., 2002. Correlation of TBM cutting performance with rock brittleness. Engineering Geology, 63:343-351.
Kahraman, S. A. I. R., Bilgin, N., Feridunoglu, C., 2003. Dominant rock properties affecting the penetration rate of percussive drills. International Journal of Rock Mechanics and Mining Sciences, 40: 711-723.
Kahraman, S., Alber, M., Fener, M., Gunaydin, O., 2010. The usability of Cerchar abrasivity index for the prediction of UCS and E of Misis Fault Breccia: regression and artificial neural networks analysis. Expert Systems with Applications, 37: 8750-8756.
Karpuz, C., Paşamehmetogˇlu, A. G., Dincer, T., Müftüoglu, Y., 1990. Drillability studies on the rotary blasthole drilling of lignite overburden series. International Journal of Surface Mining, Reclamation and Environment, 4: 89-93.
Karrari, S.S., Heidari, M., Hamidi, J.K. Sharifi Teshnizi, E., 2022. Estimation of drilling rate index values of granitic rocks with their mineralogical properties using different estimation models. Arabian Journal of Geosciences ,15: 856-865.
Kararri, S. S., Heidari, M., Sharifi Teshnizi, E., 2023. The effect of rock chipping on the penetration rate of tunnel boring machine. Journal of Rock Mechanics, 7: 23-43.
Karrari, S. S., Heidari, M., Hamidi, J. K., Teshnizi, E. S., 2024. New Cerchar device used for evaluating Cerchar abrasivity parameters. International Journal of Geomechanics, 24: 04024005.
Karrari, S. S., Heidari, M., Khademi Hamidi, J., Khaleghi-Esfahani, M., Sharifi Teshnizi, E., 2025. Estimation of Cerchar Abrasivity Index Using Petrographical, Textural and Mechanical Rock characteristics in Igneous Rocks. Geopersia, 15: 429-452.
Keller, A. M., Feng, T., Demirer, N., Darbe, R., Chen, D., 2023. Rate of penetration estimation downhole with machine learning for drilling position control. Geoenergy Science and Engineering, 224: 211593.
Ko, T.Y., Kim, T.K., Son, Y., Jeon, S., 2016. Effect of geomechanical properties on Cerchar Abrasivity Index (CAI) and its application to TBM tunnelling. Tunnelling and Underground Space Technology, 57:99-111.
Köhler, M., Maidl, U., Martak, L., 2011. Abrasiveness and tool wear in shield tunnelling in soil/Abrasivität und Werkzeugverschleiß beim Schildvortrieb im Lockergestein. Geomechanics and Tunnelling, 4: 36-54.
Koopialipoor, M., Tootoonchi, H., Jahed Armaghani, D., Tonnizam Mohamad, E., Hedayat, A., 2019. Application of deep neural networks in predicting the penetration rate of tunnel boring machines. Bulletin of Engineering Geology and the Environment, 78: 6347-6360.
Kovscek, P.D., Taylor, C.D., Thimons, E.D., 1988. Evaluation of Water-Jet Assisted Drilling with Handheld Drills. US Department of the Interior, USBM RI-9174, USA.

Lin, L., Xia, Y., Zhang, X., 2020. Wear Characteristics of TBM Disc Cutter Ring Sliding against Different Types of Rock. KSCE Journal of Civil Engineering, 24: 3145-3155.
Liu, M., Liu, X., Liu, D., Ding, C., Jiang, J., 2015. Multivariable integration method for estimating sea surface salinity in coastal waters from in situ data and remotely sensed data using random forest algorithm. Computers & geosciences, 75: 44-56.
Madhubabu, N., Singh, P. K., Kainthola, A., Mahanta, B., Tripathy, A., Singh, T. N., 2016. Prediction of compressive strength and elastic modulus of carbonate rocks. Measurement: Journal of the International Measurement Confederation, 88: 202-213.
Maitre L. E., 2002. Igneous Rocks: A Classification and Glossary of Terms 2nd edition. Recommendations of the International Union of Geological Sciences Subcommission on the Systematics of Igneous Rocks, Cambridge University, New York. 250.
McFeat-Smith, I., Fowel, R.J., 1977. Correlation of rock properties and the cutting performance of tunnelling machines. In: Proceedings of a Conference on Rock Engineering, The University of Newcastle upon Tyne, 1:581-602
Moradizadeh, M., Cheshomi, A., Ghafoori, M., TrighAzali, S., 2016. Correlation of equivalent quartz content, Slake durability index and Is50 with Cerchar abrasiveness index for different types of rock. International Journal of Rock Mechanics and Mining Sciences, 86: 42-47.
Motamed-Shariati, E., Motevalizadeh, M., Teshnizi, E. S., 2023. Estimation of rock mass deformability based on empirical relations for Ghezel Ozan dam site in the north of Iran. Quarterly Journal of Engineering Geology and Hydrogeology, 56:120-138.
Nilsen B., 2003. Investigation and testing for Norwegian hard rock TBM performance prediction. In: Bilgin N (ed) Turkiye Yeralti Kaynaklarinin Bugunu ve Gelecegi, ITU Miming Faculty 50th Year Symposium, Istanbul, Turkey, 89-96.
Nilsen B., 2003. Investigation and testing for Norwegian hard rock TBM performance prediction. In: Bilgin N (ed) Turkiye Yeralti Kaynaklarinin Bugunu ve Gelecegi, ITU Miming Faculty 50th Year Symposium, Istanbul, Turkey, 89-96.
Nisbet R., Elder J., Miner G.D., 2018. Handbook of statistical analysis and data mining applications, 2nd edition. Academic Press, 300.
Norusis M. 2002. SPSS 11.0 guide to data analysis. Prentice Hall Inc. Upper Saddle River. 350.
NTNU, 2007. Report 2B-05 drill and blast tunneling-advance rate Department of Civil and Transport Engineering, Trondheim. 250.
NTNU, 2009. Report 12C-08 rock quarrying-bench drilling. Department of Civil and Transport Engineering, Trondheim, 350.
Oliver, W.C., Pharr, G.M., 1992. An improved technique for determining hardness and elastic modulus using load and displacement sensing indentation experiments. Journal of Materials Research, 7: 1564-1583.
Omar, M., 2016. Empirical correlations for predicting strength properties of rocks-United Arab Emirates. International Journal of Geo-Engineering, 11: 248-261.
Özfırat, M. K., Yenice, H., Şimşir, F., Yaralı, O., 2016. A new approach to rock brittleness and its usability at prediction of drillability. Journal of African Earth Sciences, 119: 94-101.
Paone, J., Madson, D., 1966. Drillability studies: impregnated diamond bits (Vol. 6776). US Department of the Interior, Bureau of Mines.
Paone, J., Bruce, W. E., Virciglio, P. R., 1966. Drillability studies: statistical regression analysis of diamond drilling (No. 6880-6883). US Department of the Interior, Bureau of Mines.
Peila, D., Pelizza, S. 2009. Ground probing and treatments in rock TBM tunnel to overcome limiting conditions. Journal of mining science, 45(6), 602-619. https://doi.org/10.1007/s10913-009-0075-9
Pelizza, S., Peila, D., 2001. Rock TBM tunnelling. In Reports on Geotechnical Engineering, Soil Mechanics and Rock Engineering, Jubilee Volume in celebration of 75th anniversary of K. Terzaghi's "Erdbaumechanik" 60th Birthday of O. Univ. Prof. Dr. H. Brandl.Technische Unviversitat Wien, 5: 297-308.
Peng, J., Wong, L. N. Y., Teh, C. I., 2017. Influence of grain size heterogeneity on strength and microcracking behavior of crystalline rocks. Journal of Geophysical Research: Solid Earth, 122: 1054-1073.
Plinninger, R.J., Spaun, G., Thuro, K, 2002. Prediction and classification of tool wear in drill and blast tunnelling. Proceedings of 9th Congress of the International Association for Engineering Geology

and the Environment. Durban. South Africa. 2226-2236.
Plinninger, Ralf J., 2010. Hardrock abrasivity investigation using the Rock Abrasivity Index (RAI)." Williams, et al.,(Eds.), Geologically Active, Taylor & Francis, London. 3445-3452.
Poole, R. W., Farmer, I. W., 1978. Geotechnical factors affecting tunnelling machine performance in coal measures rock. Tunnels Tunnelling;(United Kingdom), 10:10-15.
Přikryl, R., 2006. Assessment of rock geomechanical quality by quantitative rock fabric coefficients: limitations and possible source of misinterpretations. Engineering Geology, 87: 149-162.
Rahimi, E., Sharifi Teshnizi, E., Rastegarnia, A., Motamed Al-shariati, E., 2019. Cement take estimation using neural networks and statistical analysis in Bakhtiari and Karun 4 dam sites, in south west of Iran. Bulletin of Engineering Geology and the Environment, 78: 2817-2834.
Rastegarnia, A., Teshnizi, E. S., Hosseini, S., Shamsi, H., Etemadifar, M., 2018. Estimation of punch strength index and static properties of sedimentary rocks using neural networks in south west of Iran. Measurement, 128: 464-478.
Rastegarnia, A., Lashkaripour, G. R., Sharifi Teshnizi, E., Ghafoori, M., 2021. Evaluation of engineering characteristics and estimation of static properties of clay-bearing rocks. Environmental Earth Sciences, 80: 621-630.
Ren, J., Jiang, J., Zhou, C., Li, Q., Xu, Z., 2024. Research on adaptive feature optimization and drilling rate prediction based on real-time data. Geoenergy Science and Engineering, 242:213-247.
Roduit N., 2009. JMicroVision: image analysis toolbox for measuring and quantifying components of high-definition images. Version 1.2.7. Software available for free download. http:// www. jmicrovision. Com
Rostami, J., Ghasemi, A., Alavi Gharahbagh, E., Dogruoz, C., Dahl, F., 2014. Study of dominant factors affecting Cerchar abrasivity index. Rock mechanics and rock engineering, 47: 1905-1919.
Rostami, K., Hamidi, J. K., Nejati, H. R., 2020. Use of rock microscale properties for introducing a cuttability index in rock cutting with a chisel pick. Arabian Journal of Geosciences, 13: 960-970.
Ru, Z., Zhao, H., Zhu, C., 2019. Probabilistic evaluation of drilling rate index based on a least square support vector machine and Monte Carlo simulation. Bulletin of Engineering Geology and the Environment, 78: 3111-3118.
Sadeghi, S., Teshnizi, E. S., Pash, R. R., Golian, M., 2024. Extraction of Lineaments Using Landsat Image and Digital Elevation Model: A Case Study of Zagros Orogenic Belt, West Iran. Journal of the Indian Society of Remote Sensing, 52: 2361-2373.
Sajid, M., Coggan, J., Arif, M., Andersen, J., Rollinson, G., 2016. Petrographic features as an effective indicator for the variation in strength of granites. Engineering Geology, 202: 44-54.
Shahani, N. M., Zheng, X., Wei, X., Hongwei, J., 2024. Hybrid machine learning approach for accurate prediction of the drilling rate index. Scientific Reports, 14: 24080.
Singh, T. N., Kanchan, R., Saigal, K., Verma, A. K., 2004. Prediction of p-wave velocity and anisotropic property of rock using artificial neural network technique. Journal of Scientific and Industrial Research, 63: 32-38.
Srivastava, G. K., Vemavarapu, M. M., 2021. Drillability prediction in some metamorphic rocks using composite penetration rate index (CPRI)-An approach. International Journal of Mining Science and Technology, 31: 631-641.
Streckeisen A., 1976. To each plutonic rock its proper name. Earth Sci Rev 12: 12-33.
Tabar, M.E., Katlav, M., Turk, K., 2025. Explainable ensemble algorithms with grey wolf optimization for estimation of the tensile performance of polyethylene fiber-reinforced engineered cementitious composite. Materials Today Communications, 44: p.112028.
Tanaino, A. S, 2005. Rock classification by drillability. Part I: analysis of the available classifications. Journal of Mining Science, 41: 541-549.
Tandon, R. S., Gupta, V., 2013. The control of mineral constituents and textural characteristics on the petrophysical & mechanical (PM) properties of different rocks of the Himalaya. Engineering Geology, 153: 125-143.
Telford, W.M., Geldart, L.P., Sheriff, R.E., 1990. Applied Geophysics (2nd ed.). Cambridge University Press.
Thuro, K., Spaun, G., 1996. Introducing the'destruction work'as a new rock property of toughness referring to drillability in conventional drill-and blast tunnelling. In ISRM EUROCK (pp. ISRM-EUROCK). ISRM.
Tuğrul, A., Zarif, I. H., 1999. Correlation of mineralogical and textural characteristics with engineering

properties of selected granitic rocks from Turkey. Engineering geology, 51: 303-317.
Tumac, D., Shaterpour-Mamaghan, A., Hojjati, S., Polat, C., Er, S., Copur, H., Balci, C., 2023. Determination of drilling rate index based on mineralogical and textural properties of natural stones. Bulletin of Engineering Geology and the Environment, 82: 1-18.
Ündül, Ö., 2016. Assessment of mineralogical and petrographic factors affecting petro-physical properties, strength and cracking processes of volcanic rocks. Engineering Geology, 210: 10-22.
Villeneuve M.C., 2008. Examination of geological influence on machine excavation of highly stressed tunnels in massive hard rock. Queen University Kingston, Ontario, Canada, 200.
Wang, Z., 2000. Fundamentals of Seismic Rock Physics. Elsevier, 320.
Wang, X., Zhou, L., He, M., Peng, Z., Zhang, J., 2025. XGboost with multi-feature fusion for hemodynamic state prediction. Neuroscience, 591:63-75.
Wani, S. R., Teshnizi, E. S., Jalota, S., 2025. Correlation between Cerchar abrasivity index and geotechnical properties of igneous rocks: A comprehensive analysis using machine learning algorithms and interpretative analysis. Measurement, 118989.
Wilfing, L. S. F., 2016. The Influence of Geotechnical Parameters on Penetration Prediction in TBM Tunneling in Hard Rock: Special focus on the parameter of rock toughness and discontinuity pattern in rock mass (Doctoral dissertation, Technische Universität München).
Wu, M., Liu, Z., Wang, H., Zhou, H., Wang, X., 2025. Cyclic fatigue effect on mechanical property changes of hot dry rock in wellbores of enhanced geothermal systems. International Journal of Rock Mechanics and Mining Sciences, 195: 106303.
Yang, Q., Liu, Z., Wang, X., Liu, B., Tian, F., Wang, X., 2025. Physical model test and numerical modeling of cross-sectional shape effect on evolution mechanism of time-delayed deformation and rockburst in deep tunnels. Rock Mechanics and Rock Engineering, 1-29.
Yarali, O., Kahraman, S., 2011. The drillability assessment of rocks using the different brittleness values. Tunnelling and Underground Space Technology, 26: 406-414.
Yarali, O., Soyer, E., 2013. Assessment of relationships between drilling rate index and mechanical properties of rocks. Tunnelling and underground space technology, 33: 46-53.
Yazitova, A., Yagiz, S., 2024. Performance analysis of drilling machines based on rock properties and machine's specifications. Bulletin of Engineering Geology and the Environment, 83:1-19.
Yenice H., 2019. Determination of drilling rate index based on rock strength using regression analysis. Anais da Academia Brasileira de Ciências. Annals of the Brazilian Academy of Sciences, 91: e20181095.
Yenice, H., Özdoğan, M. V., Özfırat, M. K., 2018. A sampling study on rock properties affecting drilling rate index (DRI). Journal of African Earth Sciences, 141: 1-8.
Yetkin, M. E., Özfırat, M. K., Özfırat, P. M., Elmacı, D., Yenice, H., 2025. Estimation of drilling rate index using artificial neural networks and regression analysis. Bulletin of Engineering Geology and the Environment, 84: 526-530.
Yılmaz, N. G., Goktan, R. M., Kibici, Y., 2011. Relations between some quantitative petrographic characteristics and mechanical strength properties of granitic building stones. International Journal of Rock Mechanics and Mining Sciences, 48: 506-513.
Zare, S., Bruland, A., 2013. Applications of NTNU/SINTEF drillability indices in hard rock tunneling. Rock mechanics and rock engineering. 46: 179-187.
Zhang, G. Konietzky, H., Fruhwirt, T., 2020. Investigation of scratching specific energy in the Cerchar abrasivity test and its application for evaluating rock-tool interaction and efficiency of rock cutting. Wear, 448: 203-218.
Zhou, J., Yazdani Bejarbaneh, B., Jahed Armaghani, D., Tahir, M. M., 2020. Forecasting of TBM advance rate in hard rock condition based on artificial neural network and genetic programming techniques. Bulletin of Engineering Geology and the Environment, 79: 2069-2084.
Zhou, H., Liu, Z., Shao, J., Shen, W., Hamdi, E., 2025. Effects of Stress Direction and Magnitude on Strength and Failure of Weakly Anisotropic Sandstone under True Triaxial Compression. Rock Mechanics and Rock Engineering, 1-22.
Zielesny A., 2016. From curve fitting to machine learning. Second edition, Springer, 350.